A simplified model for static/flowing dynamics in thin-layer flows of granular materials with yield

Christelle Lusso, François Bouchut, Alexandre Ern, Anne Mangeney

A simplified model for static/flowing dynamics in thin-layer flows of granular materials with yield

Christelle Lusso[1], François Bouchut[2], Alexandre Ern[1], Anne Mangeney[3,4]

[1]Université Paris-Est, CERMICS (ENPC),
F-77455, Marne-la-Vallée, France

[2]Université Paris-Est, Laboratoire d'Analyse et de Mathématiques Appliquées (UMR 8050),
CNRS, UPEM, UPEC, F-77454, Marne-la-Vallée, France

[3]Université Paris Diderot, Sorbonne Paris Cité, Institut de Physique du Globe de Paris,
Seismology group, 1 rue Jussieu, 75005 Paris, France,
[4]ANGE team, INRIA, CETMEF, Lab. J.-L. Lions, Paris, France

Abstract

We introduce a simplified model for thin-layer flows of granular materials with yield. The model is based on a viscoplastic rheology with Drucker-Prager yield stress and describes the dynamics of the velocity profile as well as the transition between static and flowing material. As opposed to most models developed to describe the static/flowing transition in thin-layer flows, the variable Z in the direction normal to the topography is conserved in our model. To evaluate the respective role of yield and viscosity in this problem, we compare both the analytical solution for the inviscid case and the numerical solution for the viscous case (with a constant viscosity or the variable viscosity of the $\mu(I)$ rheology), with experimental data. Although the model does not describe variations in the flow direction, it is able to reproduce the essential features of experiments on granular flow over an inclined static layer of grains, including the stopping time and the erosion of the initial static bed, which is shown to be closely related to the viscosity.

KEYWORDS. Granular materials, static/flowing transition, thin-layer flow, interface dynamics, velocity profile, erosion, stopping time

1 Introduction

Understanding and theoretically describing the static/flowing transition in dense granular flows is a central issue in research on granular materials, with strong implications for industry and geophysics, in particular in the study of natural gravity-driven flows. Such flows (e.g., landslides or debris avalanches) play a key role in erosion processes on the Earth's surface and represent major natural hazards. In recent years, significant progress in the mathematical, physical, and numerical modeling of gravity-driven flows has made it possible to develop and use numerical models for the investigation of geomorphological processes and assess risks related to such natural hazards. However, severe limitations prevent us from fully understanding the processes acting in natural flows and predicting landslide dynamics and deposition, see e.g., [24]. In particular, a major challenge is to accurately describe complex natural phenomena such as the static/flowing transition.

Geophysical, geotechnical, and physical studies have shown that the static/flowing transition related to the existence of no-flow and flow zones within the mass plays a crucial role in most granular flows and provides a key to understanding their dynamics in a natural context. This transition occurs in erosion-deposition processes when a layer of particles flows over a static layer or near the destabilization and stopping phases. Note that natural flows often travel over deposits of past events, which may or may not be made of the same grains,

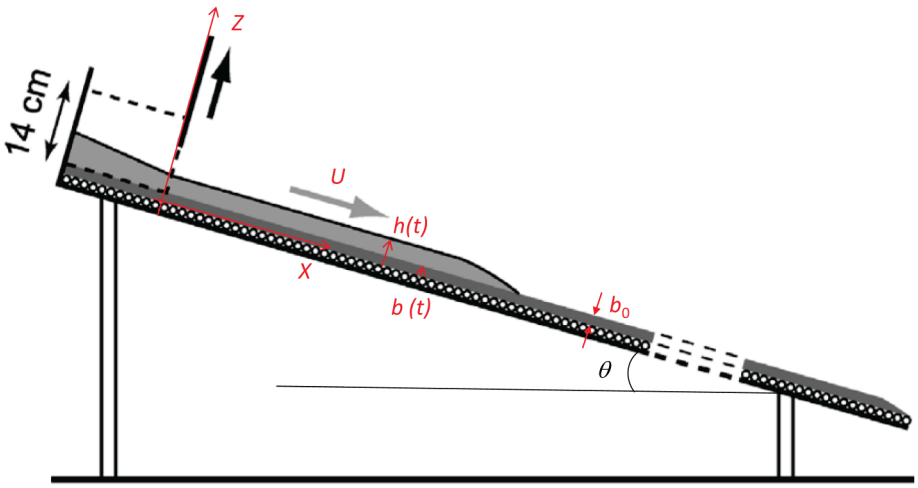

Figure 1: Experimental setup from [28] and [12] to study granular column collapse over inclined planes covered by an initially static layer made of the same grains as those released in the column. For slope angles θ a few degrees smaller than the typical friction angle δ of the involved material, a quasi-uniform flow develops behind the front.

and entrain material from the initially static bed. Even though erosion processes are very difficult to measure in the field, e.g., [7, 2, 36], entrainment of underlying material is known to significantly change the flow dynamics and deposit, e.g., [15, 34, 27, 8, 28, 30].

Experimental studies have provided some information on the static/flowing dynamics in granular flows, showing for example that the presence of a very thin layer of erodible material lying on an inclined bed may increase the maximum runout distance of a granular avalanche flowing down the slope by up to 40% and change the flow regimes [28, 17, 12]. In these experiments that mimic natural flows over initially static beds (Figure 1), quasi-uniform flows develop when the slope angle θ is a few degrees lower than the typical friction angle δ of the involved material [12]. Figures 2 and 3 show new data extracted from the experiments performed by [12] on the change with time of the static/flowing interface position b and the velocity profiles $U(Z)$ within the granular mass, where Z is the direction normal to the bed. At a given position X along the plane, the flow is shown to excavate the initially static layer immediately when the front reaches this position. The static/flowing interface rapidly penetrates into the static layer, stabilizing at an almost constant value for significantly high slopes and then rising linearly or exponentially toward the free surface until the whole mass of material stops (Figure 2). A theoretical description of these observations is still lacking. In particular, questions remain as to what controls the change with time of the static/flowing interface position and the velocity profiles and how these characteristics are related to the rheology of the granular material and the initial and boundary conditions.

In order to alleviate the high computational costs required to describe the real topography and the rheology, both of which play a key role in natural flow dynamics, thin-layer (i.e., the thickness of the flow is assumed to be small compared to its downslope extension) depth-averaged models are generally used to simulate landslides [32]. Such models have been rigorously derived for arbitrary topography, but the static/flowing transition is generally

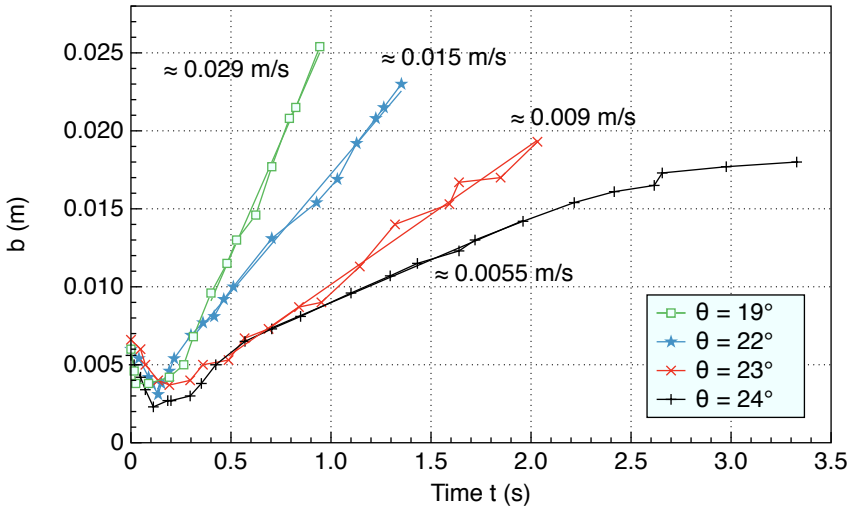

Figure 2: Position of the static/flowing interface b as a function of time t until the granular mass stopes, measured at $X = 90$cm from the gate, from experiments of granular collapse over an initially static granular layer of thickness $b^0 = 5$mm on an inclined channel of slope angle $\theta = 19^o$ (green squares), $\theta = 22^o$ (blue stars), $\theta = 23^o$ (red crosses), and $\theta = 24^o$ (black vertical crosses). Time $t = 0$s corresponds to the time when the front of the flowing layer reaches the position $X = 90$cm. The approximate upward velocity $\dot{b}$ of the static/flowing interface is indicated in m/s for each slope angle. These new results have been extracted from the experiments performed by [12] and [13] for granular columns of initial radius $r_0 = 20$cm, initial thickness $h_0 = 14$cm, and width $W = 20$cm (i.e., volume $V = 5600\text{cm}^3$).

neglected, e.g., [4, 3, 29]. Several attempts have been made to describe this transition in thin-layer (i.e., shallow) models, in particular by deriving an equation for the static/flowing interface position or by establishing erosion/deposition rates, e.g., [22, 18]. However, these approaches are generally based on debatable phenomenological laws and/or are too schematic to be extended to natural flows [19]. In particular, the simplifications used in some previous models lead to an inconsistent energy equation [5]. A better understanding of the non-averaged case is necessary to define more physically relevant depth-averaged models including the static/flowing transition. As a first step in this direction, we focus here on non-averaged thin-layer models.

Recent work has shown that viscoplastic flow laws with yield stress well describe granular flows and deposits in different regimes from steady uniform flows [14, 33, 20, 21] to transient granular collapse over rigid or erodible horizontal beds [9, 23] and inclined beds [16]. Very good agreement with experiments is obtained even though these laws, and in particular the so-called $\mu(I)$ rheology, where I is the inertial number [21], have been shown to be ill-posed in the quasi-static regime, i.e., for small I (and also for large I) [1]. These promising results may be related to the use of a coarse mesh, whereby simulations avoid the ill-posedness by damping the fast-growing high wavenumbers. In any case, the quasi-static regime near the static/flowing interface is known to be very complex, involving strong and weak force chains and local rearrangement of particles, e.g., [10, 31]. This regime is not accurately described by the proposed viscoplastic laws involving a simple yield stress. Questions however remain as to whether such 'simple' viscoplastic laws are able to describe quantitatively the change with time of the static/flowing interface position and the velocity profiles observed experimentally for flows over an initially static bed and how the viscosity affects these processes. An analytic expansion in the shallow regime from such a viscoplastic model with yield stress has been performed in [6], giving a theoretical basis for equations on the static/flowing interface dynamics in a dry granular material.

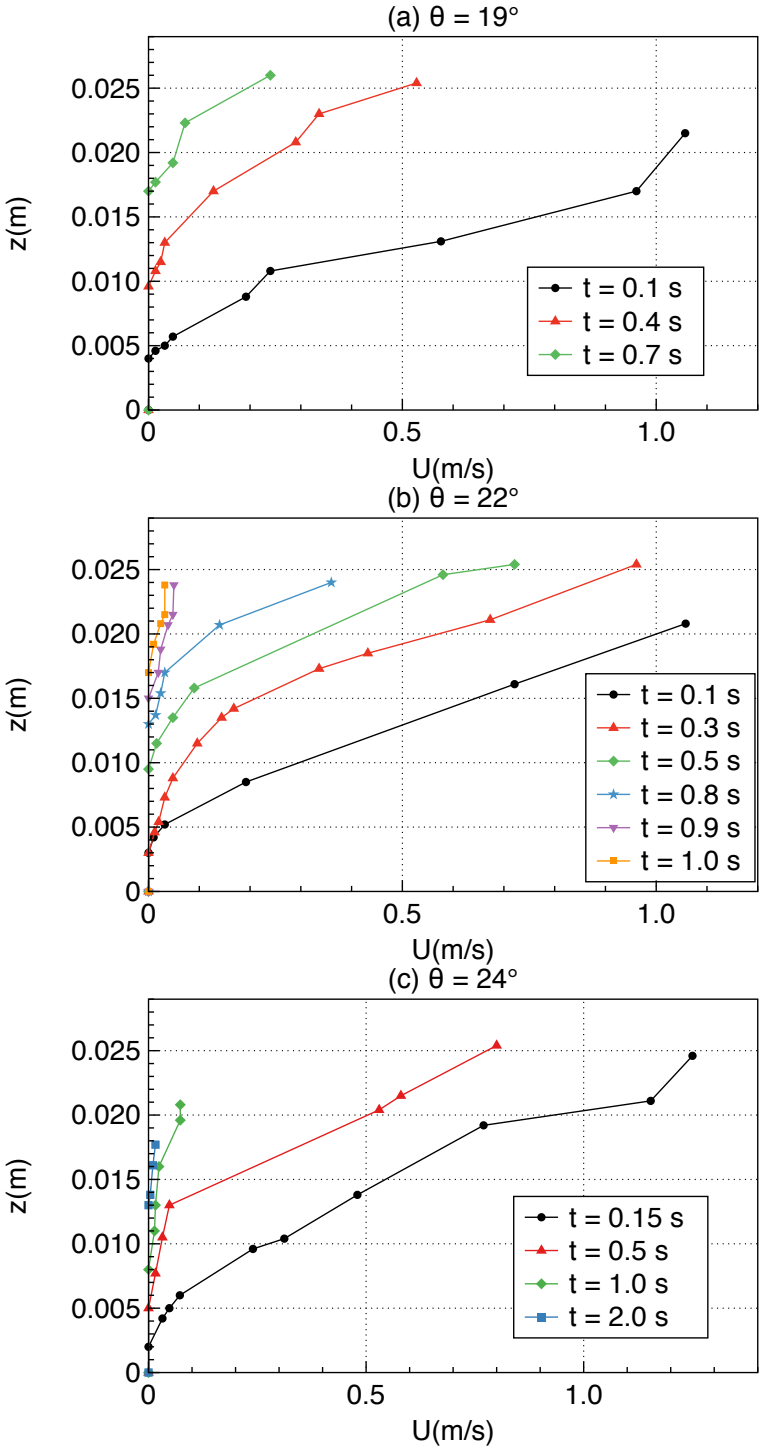

Figure 3: Velocity profiles $U(Z)$ at different times until the granular mass stops, measured at $X =$ 90cm from the gate, in experiments of granular collapse over an initially static granular layer of thickness $b^0 = 5$mm on an inclined channel of slope angle (a) $\theta = 19^o$, (b) $\theta = 22^o$, and (c) $\theta = 24^o$. Time $t = 0$s corresponds to the time when the front of the flowing layer reaches the position $X = 90$cm. These new results have been extracted from the experiments performed by [12] and [13] for granular columns of initial radius $r_0 = 20$cm, initial thickness $h_0 = 14$cm, and width $W = 20$cm (i.e., volume $V = 5600\text{cm}^3$).

We propose here to evaluate the dynamics produced by the mathematical model of [6], for a simplified case in which we remove the flow-parallel variable X that is present in [6]. Although this variable X plays a key role in real flows, taking into account the fluctuations of the free surface, topography and inflow information, we can neglect it at this initial stage. Thus, we assume here a uniform flow ($h = cst$) over a flat inclined plane ($\theta = cst$). We show that the analysis of this simple shear system provides new insight into the change with time of the static/flowing interface position and the velocity profiles.

A key point in our model that fundamentally differs from previous thin-layer models (see [19] for a review) is that even if the flow is assumed to be shallow, the normal variable Z is still present. The formulation involves an extra boundary condition at the static/flowing interface $Z = b(t)$ that determines its time evolution. The effects of gravity and internal friction are taken into account via a source term S. The model is introduced in Section 2. Then, in Section 3, we derive an analytical solution for the inviscid case with a constant source term, which partly reproduces the experimental observations and shows explicitly how the static/flowing interface position and the velocity profiles are related to the flow characteristics and to the initial and boundary conditions. In Section 4, we introduce two new numerical methods for the simulation of the viscous model, with a constant viscosity or the variable viscosity associated with the $\mu(I)$ rheology. The numerical results show that, as opposed to the inviscid case, viscosity makes it possible to reproduce the initial penetration of the static/flowing interface within the static bed and the exponential shape of the velocity profiles near this interface. Finally, in Section 5, these results are discussed based on comparison with former experimental and numerical studies on granular flows, showing the key features and the limits of this shallow viscoplastic model for providing a better understanding and modeling of laboratory and natural flows.

2 A simplified model with source term and moving static/flowing interface

2.1 Origin of the model

A shallow model for viscoplastic flows with yield stress and static/flowing transition has been derived in [6]. It is formulated in the variables X in the direction tangent to the topography, and Z normal to it. The topography is described by its angle $\theta(X)$ with the horizontal (Figure 4 in the case of a flat topography). The starting governing equations are the dynamics of an incompressible viscoplastic flow with Drucker–Prager yield stress, characterized by the rheological law

$$\boldsymbol{\sigma} = -p\,\mathrm{I}d + 2\nu D\mathbf{U} + \mu_s p\,\frac{D\mathbf{U}}{\|D\mathbf{U}\|}, \tag{2.1}$$

where $\boldsymbol{\sigma}$ is the stress tensor (normalized by the density) p is the scalar pressure (also normalized by the density), $D\mathbf{U}$ is the strain rate tensor $D\mathbf{U} = (\nabla\mathbf{U} + (\nabla\mathbf{U})^t)/2$ with $\mathbf{U}$ the velocity vector. Here the norm of a matrix $A = (A_{ij})$ is $\|A\| = (\frac{1}{2}\sum_{ij} A_{ij}^2)^{1/2}$. The coefficients $\mu_s > 0$ and $\nu \geq 0$ are the internal friction and the kinematic viscosity, respectively. Under the assumptions that the width of the layer, the curvature of the topography, and the viscosity are small, the internal friction angle is close to the slope angle, the velocity is small, and the pressure is convex with respect to the normal variable Z, a formal expansion of the governing equations leads to the momentum balance equation

$$\partial_t U + S - \partial_Z\big(\nu\partial_Z U\big) = 0 \quad \text{for all } Z \in (b, h), \tag{2.2}$$

where $U(t, X, Z)$ is the velocity in the direction tangent to the topography. The kinematic viscosity ν is taken constant here, but another choice deduced from the so called $\mu(I)$ rheology is evaluated in Subsection 4.5. In (2.2), $h(t, X)$ is the thickness of the layer, and $b(t, X)$ is the position of the interface between the static part $Z < b(t, X)$ (where we set $U \equiv 0$) and

the flowing part $Z > b(t, X)$. The thickness h evolves according to a kinematic free-surface condition (not written here), and the evolution of the interface b is implicitly governed by the boundary conditions for all $t > 0$,

$$U = 0 \quad \text{at } Z = b, \tag{2.3a}$$
$$\nu \partial_Z U = 0 \quad \text{at } Z = b, \tag{2.3b}$$
$$\nu \partial_Z U = 0 \quad \text{at } Z = h. \tag{2.3c}$$

Knowing that the material is at rest in the part below the interface, these boundary conditions mean that the velocity is continuously differentiable through the interface (in the viscous case), and that the viscous stress vanishes at the free surface $Z = h$.

The source S in (2.2) depends on t, X, Z and is expressed as

$$S = g(-\sin\theta + \partial_X(h\cos\theta)) - \mu_s \partial_Z p \quad \text{for all } Z \in (b, h), \tag{2.4}$$

where $g > 0$ is the gravity acceleration, $\mu_s = \tan\delta > 0$ is the friction coefficient with δ the friction angle related to the material, and $p(t, X, Z)$ is the pressure. This pressure has an asymptotic nonlinear expression in terms of $\partial_X U$ and $\partial_Z U$, but the particular form of this expression is irrelevant here. The formula (2.4) is valid in the context of positive angle θ (note that this convention differs from [6]) and of a (strictly) increasing velocity profile in the flowing layer, i.e., $\partial_Z U > 0$ for all $Z \in (b, h)$.

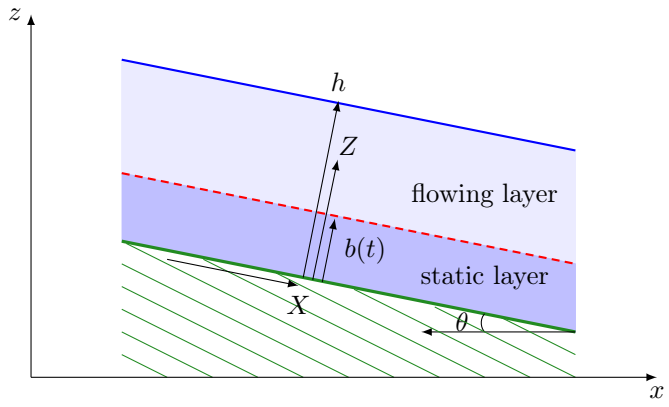

Figure 4: Simplified flow configuration consisting of a uniform flowing layer over a uniform static layer, both parallel to the rigid bed of slope angle θ. The static/flowing interface position is $b(t)$, and the total thickness of the mass h is constant.

2.2 The simplified model

The motivation of our simplified model stems from the fact that the system (2.2), (2.3) involves the dependency on X of the unknowns only via the thickness of the layer h and the source term S, or equivalently via the expression of the pressure, because of (2.4). In other words, if the source S and the thickness of the layer h are known, the system (2.2), (2.3) can be considered as a system in the variables t, Z, while X is only a parameter.

Therefore, our simplified model with moving interface considers that (at fixed X, and we thus omit the variable X) the source is given empirically as a function $S(t, Z)$. The angle $\theta > 0$ is then constant, and we assume also that h is independent of time, and therefore constant. Our system reduces then to finding $U(t, Z)$ for $b(t) < Z < h$, and $b(t)$ satisfying $0 < b(t) < h$, such that

$$\partial_t U(t, Z) + S(t, Z) - \partial_Z\big(\nu \partial_Z U(t, Z)\big) = 0 \quad \text{for all } Z \in (b(t), h), \tag{2.5}$$

with the boundary conditions for all $t > 0$,

$$U = 0 \quad \text{at } Z = b(t), \tag{2.6a}$$
$$\nu \partial_Z U = 0 \quad \text{at } Z = b(t), \tag{2.6b}$$
$$\nu \partial_Z U = 0 \quad \text{at } Z = h. \tag{2.6c}$$

We assume that $S(t, Z)$ is defined for $Z \in [0, h]$ and is continuous in time and space. Finally, we specify a continuous velocity profile $U^0(Z)$ defined for $Z \in [0, h]$, such that for some $b^0 \in (0, h)$ (initial position of the interface), the function U^0 satisfies $U^0(Z) = 0$ for $Z \in [0, b^0]$, and $\partial_Z U^0 > 0$ for $Z \in (b^0, h)$. The initial condition on the velocity is then formulated as

$$U(0, Z) = U^0(Z) \quad \text{for all } Z \in [0, h], \tag{2.7}$$

where $U(0, Z)$ is the limit as $t \downarrow 0$ of $U(t, Z)$ extended by 0 for $Z < b(t)$.

We remark that if we take an hydrostatic pressure $p = g \cos\theta (h - Z)$ in (2.4), neglecting the derivative in X (we recall that X has been considered as a parameter, which does not mean that the quantities are independent of X), we infer that S is constant in time (and uniform in space) with

$$S = g(-\sin\theta + \mu_s \cos\theta). \tag{2.8}$$

The source term is thus the result of the balance between the driving force due to gravity ($g \sin\theta > 0$) and the friction force ($\mu_s g \cos\theta > 0$). Indeed, in the case of (2.8), according to [6], the solution of the system (2.5), (2.6), (2.7) is an exact solution to the two-dimensional original viscoplastic model without dependency in X.

2.3 Properties of the model

The simplified model (2.5), (2.6), (2.7) enjoys several interesting properties; for more insight into their proof, we refer to [25]. We make the assumptions stated in Subsection 2.2 on the initial data.

- Monotonicity of the velocity profile. Assume that $\nu > 0$ and that the source term is decreasing in space

$$\partial_Z S(t, Z) \leq 0 \quad \text{for all } t \geq 0, \text{ and all } Z \in [0, h]. \tag{2.9}$$

  Condition (2.9) can be interpreted as a stability condition. Recalling (2.4), this condition can also be stated as a convexity property for the pressure, i.e., $\partial^2_{ZZ} p \geq 0$. The stability condition (2.9) is obviously satisfied if the source term is uniform in space. Then, under the above assumptions, for all $t \geq 0$, and as long as $0 < b(t) < h$, the following holds:

$$\partial_Z U(t, Z) > 0 \quad \text{for all } Z \in (b(t), h). \tag{2.10}$$

  Moreover, the source term is nonnegative at the interface

$$S(t, b(t)) \geq 0 \quad \text{for all } t > 0. \tag{2.11}$$

  This last property is obtained by differentiating (2.6a) with respect to time, which yields

$$\partial_t U(t, b(t)) + \partial_Z U(t, b(t)) \dot{b}(t) = 0. \tag{2.12}$$

  Since $\nu \neq 0$, the condition (2.6b) leads to $\partial_t U(t, b(t)) = 0$. Then, evaluating (2.5) at $Z = b(t)$, we infer that

$$S(t, b(t)) = \nu \partial^2_{ZZ} U(t, b(t)). \tag{2.13}$$

  Owing to (2.10) and using again (2.6b), we obtain $\partial^2_{ZZ} U(t, b(t)) = \lim_{Z \downarrow b(t)} \partial_Z U(t, Z)/(Z - b(t)) \geq 0$, whence the result (2.11).

In the case $\nu = 0$, we impose (2.11) as an additional condition in the simplified model. This additional condition can be interpreted as an entropy condition in the limit of vanishing viscosity.

We observe that in the case (2.8) of constant source, the condition (2.11) implies that $\tan\theta \leq \mu_s$, saying that the internal friction must at least neutralize the gravity force due to the slope. This is a necessary condition for a solution to the model with moving interface (2.5), (2.6), (2.7) to exist. Indeed, if this condition is not satisfied, we expect that "$b = 0$", meaning that all the layer flows down.

- We can formally derive a differential equation for the time evolution of the position of the interface.
  If $\nu > 0$ and $S(t, b(t)) \neq 0$, then

$$\dot{b}(t) = \left(\frac{\partial_Z S(t, b(t)) - \nu \partial^3_{ZZZ} U(t, b(t))}{S(t, b(t))} \right) \nu. \tag{2.14}$$

  This differential equation can be obtained by differentiating (2.6b) with respect to time, using (2.13), and evaluating the derivative with respect to Z of (2.5) at $Z = b(t)$.
  If $\nu = 0$ and $\partial_Z U(t, b(t)) \neq 0$, then

$$\dot{b}(t) = \frac{S(t, b(t))}{\partial_Z U(t, b(t))}, \tag{2.15}$$

  this identity being deduced from (2.12), and (2.5) evaluated at $Z = b(t)$.

  These formulas show the strong interrelation between the velocity profile in the direction perpendicular to the inclined plane and the evolution of the static/flowing interface position.

3 Analytical solution in the inviscid case with a constant and uniform source term

3.1 Analytical solution

In the inviscid case $\nu = 0$, the simplified model (2.5), (2.6), (2.7) can be written

$$\partial_t U(t, Z) + S(t, Z) = 0 \quad \text{for all } Z \in (b(t), h), \tag{3.1}$$

with the boundary condition for all $t > 0$,

$$U(t, b(t)) = 0, \tag{3.2}$$

the initial condition (2.7), and the entropy condition (2.11). Moreover, if the source term is chosen constant and uniform as in (2.8), i.e.,

$$S(t, Z) = S := g \cos\theta (\tan\delta - \tan\theta) \geq 0, \tag{3.3}$$

with $\mu_s = \tan\delta$, $\theta \leq \delta$, then we can infer an analytical solution. Specifically, the solution to (3.1), (3.2), (2.7) is given by

$$U(t, Z) = \max\Big(U^0(Z) - St, 0 \Big) \quad \text{for all } Z \in [0, h]. \tag{3.4}$$

Equation (3.4) shows that the velocity profile (at all times when a flowing layer exists) has the same shape as the initial velocity profile: it is just shifted towards decreasing velocities with a constant speed S, and clipped below the value 0. Note that the velocity profile only depends on g, θ, δ through S in (3.3). If $S = 0$, the solution is steady, while if $S > 0$,

the velocity decreases with time, until the stopping of the flow. Furthermore, the interface position $b(t)$ results from the following implicit equation:

$$U^0(b(t)) = St. \tag{3.5}$$

This equation has a unique solution in $[b^0, h]$ for all times $t \leq t^{\text{stop}}$, with t^{stop} the time when the whole mass stops, defined by

$$t^{\text{stop}} = \frac{U^0(h)}{S} = \frac{U^0(h)}{g\cos\theta(\tan\delta - \tan\theta)}. \tag{3.6}$$

The complete stopping of the flow occurs at $t = t^{\text{stop}}$. For all times $t > t^{\text{stop}}$, the velocity U can be extended by setting $U(t, Z) = 0$ for all $Z \in [0, h]$, and $b(t) = h$.

3.2 Choice of the parameters and initial conditions

In order to compare the analytical solution to the results presented in Figures 2 and 3 extracted from the experiments performed by [12], we have to prescribe the friction angle δ, the slope angle θ, the thickness of the granular layer h, the thickness of the initially static layer b^0, and the initial velocity profile $U^0(Z)$. Glass beads of diameter $d = 0.7$mm were used, with repose and avalanche angles of about 23^o and 25^o, respectively. Because wall effects are known to increase the effective friction for granular flows in channels as those of [12], we use here a friction angle of $\delta = 26^o$ [35, 20, 16]. We perform different tests by varying the slope angle θ from 19^o to 24^o, while we prescribe $b^0 = 5$mm, which is the initial static width in the experiments, and $h = 0.02$m, corresponding to the mean thickness at the position $X = 90$cm where the measurements have been performed, see Figure 3. Thus unless specified, we always take

$$\delta = 26^o, \qquad b^0 = 0.005\text{m}, \qquad h = 0.02\text{m}. \tag{3.7}$$

The objective here is only to compare the order of magnitude and the general trend of the analytical solution to the experimental results, since the experiments are more complicated than the uniform granular layer and the initial conditions prescribed in the model. In particular, the thickness of the granular layer in the experiments may vary by up to 20% during the flow and slightly depends on the inclination angle (see Figure 3). Furthermore, the initial velocity profiles and the maximum velocity also depend on the inclination angle, while we impose here the same velocity profile for all the tests.

Velocity profiles in experimental granular flows have been extensively measured in very different regimes, see e.g., [14]. For free surface flows over rigid inclined beds, the velocity profiles vary with inclination, thickness of the flow, and time. Essentially, the velocity profiles may vary from a linear profile for thin layers over small slope angles to Bagnold-like profiles for higher inclinations. The same general trend is observed for thicker flows (see Figure 5 of [14]). For surface flows over a pile of static grains, the velocity profiles roughly exhibit an upper linear part in the flowing layer and a lower exponential tail near the static/flowing interface (see Figure 6 of [14]). This is consistent with the measurements shown in Figure 3. Furthermore, experimental results suggest that the shear rate $\partial_Z U$ is almost constant and equal to $0.5\sqrt{\frac{g}{d}}$ (see e.g., equation (11) of [14]). As a result, for a linear profile of slope α_1 (see case (a) below), we choose $\alpha_1 = 70\text{s}^{-1}$, which is consistent with the velocity profiles measured at $t = 0$s in Figure 3.

In order to investigate the different possible profiles of the velocity, we choose three initial velocity profiles defined, for all $Z \in [b^0, h]$, as:

(a) linear profile $U^0(Z) = \alpha_1(Z - b^0)$, with $\alpha_1 = 70\text{s}^{-1}$,

(b) exponential profile $U^0(Z) = \alpha_2(e^{\beta Z} - e^{\beta b^0})$, with $\alpha_2 = 0.1\text{ms}^{-1}$ and $\beta = 130\text{m}^{-1}$,

(c) Bagnold profile $U^0(Z) = \alpha_3((h - b^0)^{\frac{3}{2}} - (h - Z)^{\frac{3}{2}})$, with $\alpha_3 = 545\text{m}^{-1/2}\text{s}^{-1}$.

In each case, the maximum velocity is $U^0(h) \simeq 1\text{ms}^{-1}$. For each profile, equation (2.15) provides explicitly the time evolution of the static/flowing interface position as follows:

(a) $b(t) = \dfrac{S}{\alpha_1}t + b^0$,

(b) $b(t) = \dfrac{1}{\beta}\log\left(\dfrac{S}{\alpha_2}t + e^{\beta b^0}\right)$,

(c) $b(t) = h - \left((h-b^0)^{3/2} - \frac{S}{\alpha_3}t\right)^{2/3}$.

These formulae are valid as long as $t \leq t^{\text{stop}} = U^0(h)/S$, i.e., $b(t) \leq h$.

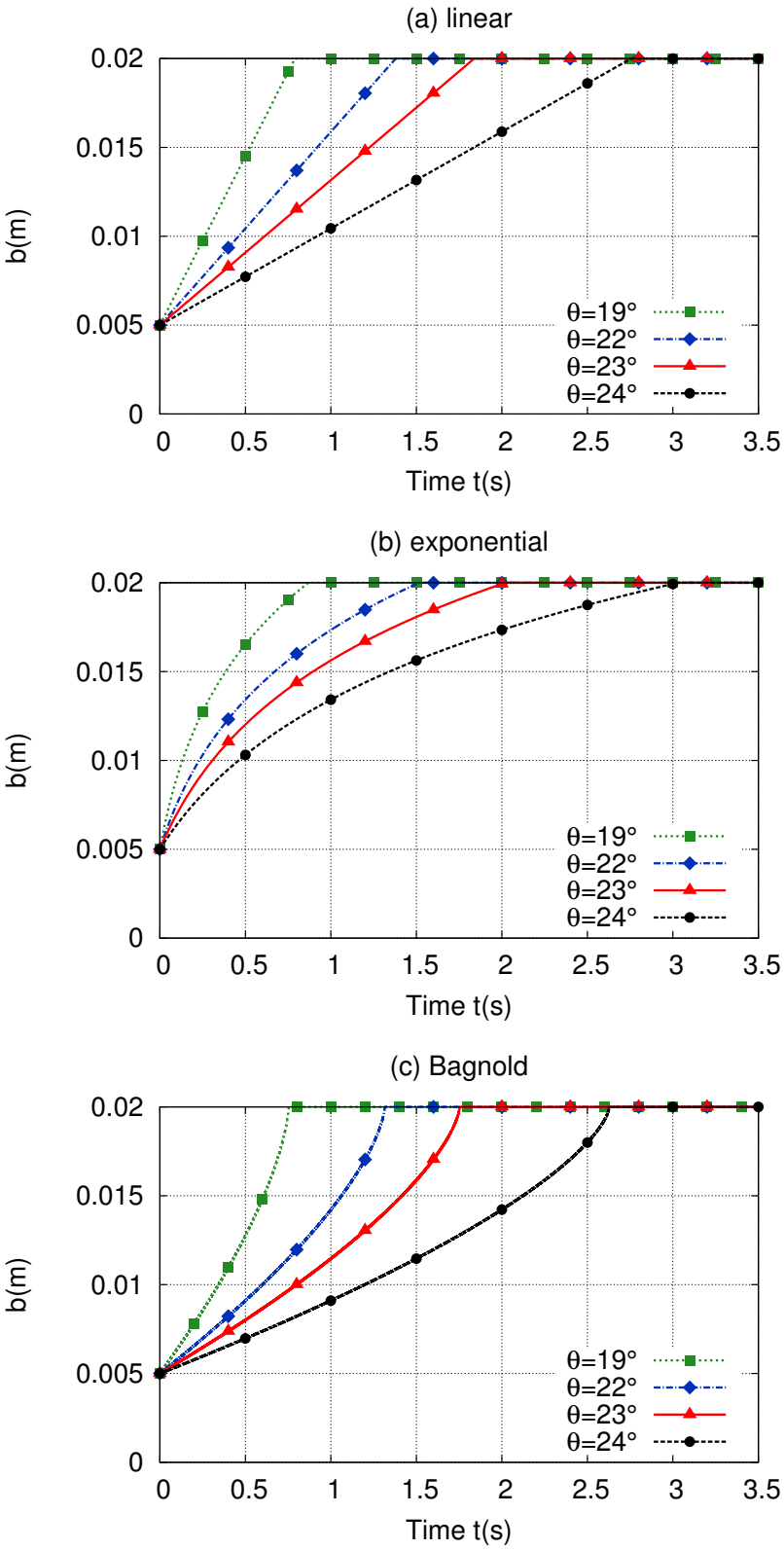

Figure 5: Static/flowing interface position b as a function of time t in the inviscid case, for different slope angles and for an initially static granular layer of thickness $b^0 = 5$mm, using (a) a linear, (b) an exponential, and (c) a Bagnold initial velocity profile.

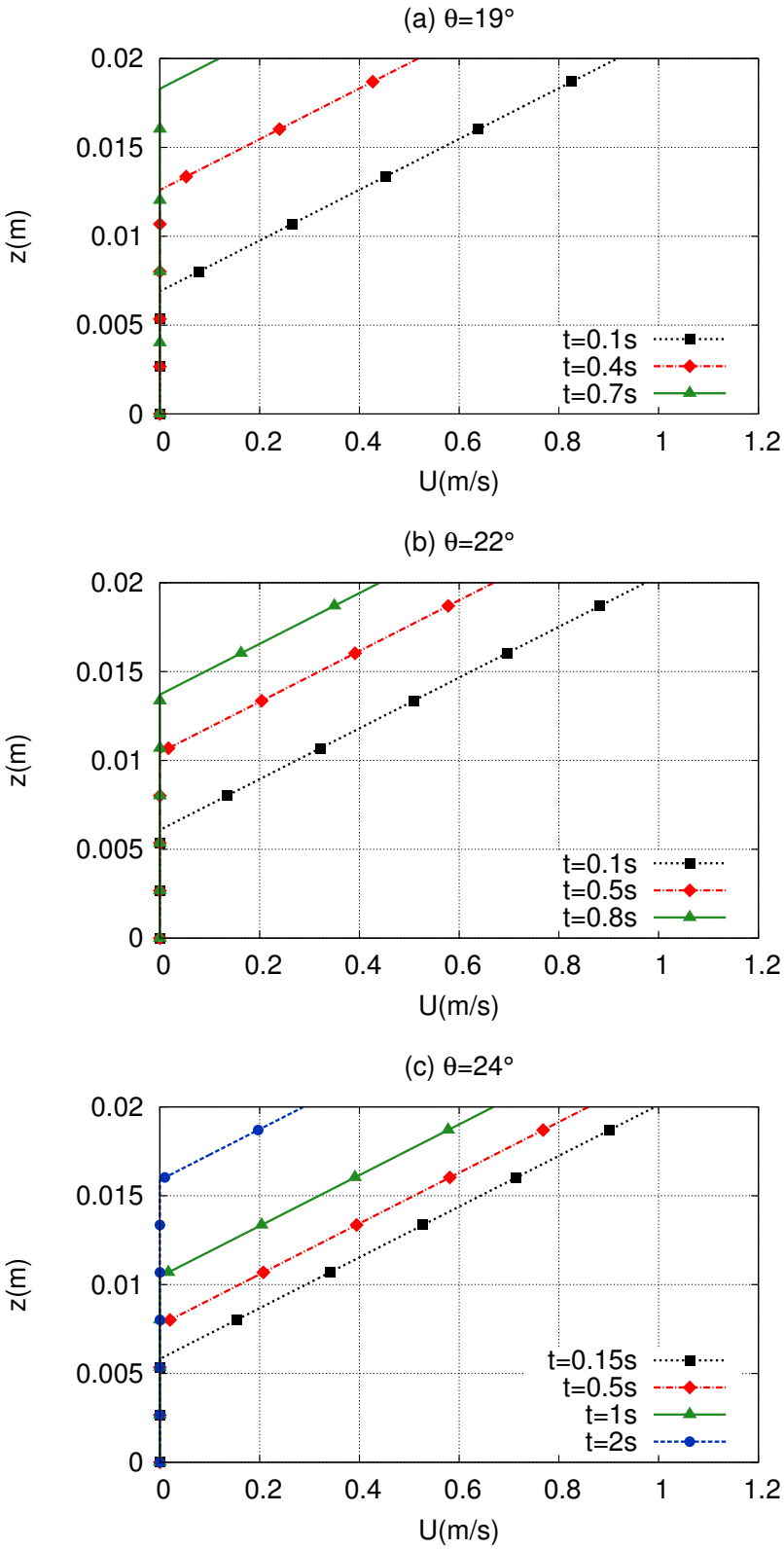

Figure 6: Velocity profiles $U(Z)$ at different times in the inviscid case, with a linear initial velocity profile and an initially static granular layer of thickness $b^0 = 5$mm over an inclined plane of slope (a) $\theta = 19^o$, (b) $\theta = 22^o$, and (c) $\theta = 24^o$.

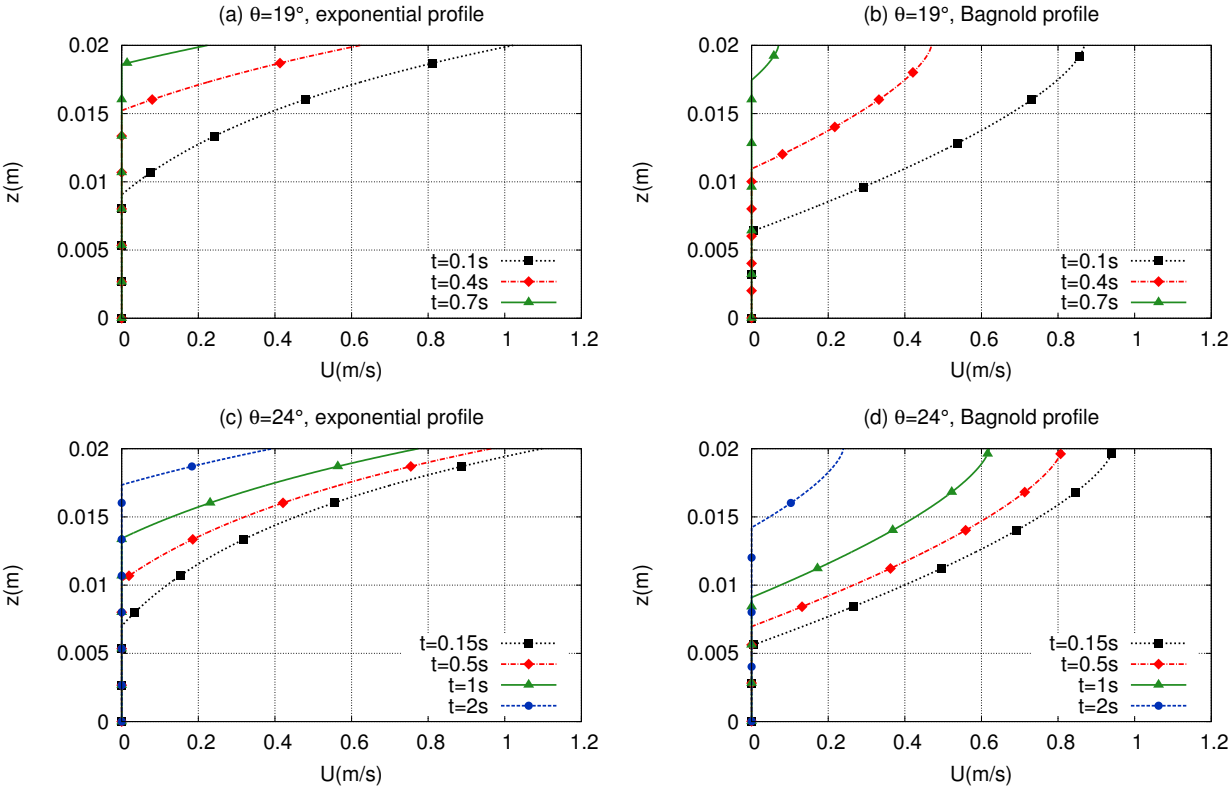

Figure 7: Velocity profiles $U(Z)$ at different times in the inviscid case, with an initially static granular layer of thickness $b^0 = 5$mm over an inclined plane of slope (a,b) $\theta = 19^o$ and (c,d) $\theta = 24^o$, using (a,c) an exponential and (b,d) a Bagnold initial velocity profile.

3.3 Results and comparison with experiments

The $b(t)$ curves are plotted in Figure 5 and the $U(Z)$ profiles in Figures 6 and 7. The evolution of the static/flowing interface position $b(t)$ obtained from the analytical solution (Figure 5) reproduces to a certain extend the experimental observations (Figure 2). The shape of $b(t)$ is directly related to the velocity profile, as demonstrated by equation (2.15). For the analytical solution, depending on the initial velocity profile, the stopping time is in the range 2.75-3s for $\theta = 24^o$, 1.35-1.5s for $\theta = 22^o$, and 0.75-0.85s for $\theta = 19^o$, while $t^{\text{stop}} \simeq 3.4$s, $t^{\text{stop}} \simeq 1.4$s, and $t^{\text{stop}} \simeq 0.9$s in the experiments, respectively. As a result, the stopping time is well reproduced by the analytical solution, even though its strong increase for $\theta = 24^o$ is underestimated in the analytical solution. On the other hand, the penetration of the static/flowing interface within the initially static bed is not reproduced by the analytical solution that instead predicts a static/flowing interface rising towards the free surface at all times.

The decrease of the velocity with time is relatively well reproduced up to about 0.8s. With the analytical solution, the velocity profiles maintain the same shape while the maximum velocity decreases, as observed in the experiments. The decrease of the maximum velocity in the experiments and with the analytical solution are very similar (Figures 3 and 7). At later times ($t \geq 1$s) and at $\theta = 22^o$ and $\theta = 24^o$, the experiments show a clear change in the velocity profile (see Figure 3c at $t = 1$s and $t = 2$s) that is not reproduced by the constant shape of the velocity profiles predicted by the analytical solution. Furthermore, the maximum velocity decreases much faster in the experiments. In the experiments, the velocity profiles seem to be closer to linear for smaller slopes ($\theta = 19^o$ and $\theta = 22^o$) and more exponential for $\theta = 24^o$. Referring to equation (3.5) and Figure 5, this may explain why $b(t)$ measured experimentally (Figure 2) has an exponential shape at $\theta = 24^o$, while it is closer to linear for

smaller slope angles.

4 Numerical solution to the viscous model

In this section, we compare a numerical solution for our simplified model (2.5), (2.6), (2.7) with viscosity $\nu > 0$ and constant and uniform source term S given by (3.3), to the experimental data.

Our model being formulated under an unusual form, we introduce two numerical methods. They both involve quite elementary tools, but are effective and give very similar results. Note that our several tries to use the differential equation (2.14) in a numerical method led to instabilities (not presented), thus the two methods described here avoid doing that. We describe the main features of the transient regime by a scale analysis. The comparison to experiments is finally performed, first with constant viscosity, then with variable viscosity deduced from the $\mu(I)$ viscoplastic rheology.

4.1 Discretization by moving interface

The first numerical method hinges on the rewriting of (2.5), (2.6), (2.7) in a normalized coordinate $0 \leq Y \leq 1$. We perform the change of variables

$$t = \tau, \qquad Z = b(\tau) + (h - b(\tau))Y, \tag{4.1}$$

that leads to the differential relations $\partial_\tau = \partial_t + \dot{b}(\tau)(1-Y)\partial_Z$ and $\partial_Y = (h-b(\tau))\partial_Z$. Here, ∂_t and ∂_τ denote the differentiation with respect to time at constant Z and Y, respectively. The change of variables (4.1), and hence the discretization method presented in this subsection, is appropriate as long as there is a flowing layer. Another discretization method dealing with the stopping phase when $b(t)$ reaches the total height h, is presented in Subsection 4.2. The discretization method considered in this subsection has the advantage of tracking explicitly the position of the static/flowing interface, while the method of Subsection 4.2 requires a post-processing to evaluate the interface position.

Using the change of variables (4.1), equation (2.5) is transformed into

$$\partial_\tau U - \dot{b}\frac{1-Y}{h-b}\partial_Y U + S - \frac{\nu}{(h-b)^2}\partial^2_{YY} U = 0 \quad \text{for all } Y \in (0,1), \tag{4.2}$$

and the boundary conditions (2.6) into

$$U = 0 \quad \text{at } Y = 0, \tag{4.3a}$$

$$\nu\partial_Y U = 0 \quad \text{at } Y = 0, \tag{4.3b}$$

$$\nu\partial_Y U = 0 \quad \text{at } Y = 1. \tag{4.3c}$$

We split the space domain $(0,1)$ in n_Y cells of length ΔY with $n_Y \Delta Y = 1$, and denote by $Y_j = (j - 1/2)\Delta Y$, for all $j = 1 \dots n_Y$ the center of the cells. The discrete times t^n, for $n \geq 0$ are related by $t^{n+1} = t^n + \Delta t^n$, where Δt^n is the time step (chosen according to the CFL condition (4.7) below) and $t^0 = 0$. We write a finite difference scheme for the discrete unknowns $U_j^n \simeq U(t^n, Y_j)$ and $b^n \simeq b(t^n)$, for all $j = 1 \dots n_Y$ and all $n \geq 1$, using the initial conditions on U^0 (and b^0) to initialize the scheme. For all $n \geq 0$, given $(U_j^n)_{1\leq j\leq n_Y}$ and b^n, the equations to compute $(U_j^{n+1})_{1\leq j\leq n_Y}$ and b^{n+1} are

$$\frac{U_j^{n+1} - U_j^n}{\Delta t^n} - \frac{(1-Y_j)}{h-b^n}a_j^{n+\frac{1}{2}} + S(t^n, Y_j) - \frac{\nu}{(h-b^n)^2}\frac{U_{j+1}^{n+1} + U_{j-1}^{n+1} - 2U_j^{n+1}}{\Delta Y^2} = 0, \tag{4.4}$$

for all $j = 1 \dots n_Y$, with

$$a_j^{n+\frac{1}{2}} = \begin{cases} \dot{b}^{n+\frac{1}{2}}\dfrac{U_j^n - U_{j-1}^n}{\Delta Y} & \text{if } \dot{b}^{n+\frac{1}{2}} \leq 0, \\ \dot{b}^{n+\frac{1}{2}}\dfrac{U_{j+1}^n - U_j^n}{\Delta Y} & \text{if } \dot{b}^{n+\frac{1}{2}} \geq 0, \end{cases} \quad \text{with } \dot{b}^{n+\frac{1}{2}} = \frac{b^{n+1} - b^n}{\Delta t^n}, \tag{4.5}$$

together with the boundary conditions

$$U_0^{n+1} = -U_1^{n+1}, \tag{4.6a}$$
$$U_0^{n+1} = U_1^{n+1}, \tag{4.6b}$$
$$U_{n_Y+1}^{n+1} = U_{n_Y}^{n+1}. \tag{4.6c}$$

Equations (4.6a) and (4.6c) are used to provide the ghost values U_0^{n+1} and $U_{n_Y+1}^{n+1}$ involved in (4.4) for $j = 1$ and $j = n_Y$, while equation (4.6b) is used to determine b^{n+1} as described below. We observe that in (4.4), the diffusive term is treated implicitly in time, while the first-order derivative of U is treated explicitly using upwinding. As a result, we impose the CFL condition

$$\frac{\Delta t^n |\dot{b}^{n+\frac{1}{2}}|}{h - b^n} \leq \Delta Y. \tag{4.7}$$

This CFL condition is evaluated approximately using the value $\dot{b}^{n-\frac{1}{2}}$ from the previous time step, since $\dot{b}^{n+\frac{1}{2}}$ is unknown at the beginning of the time step; for $n = 0$, the value 0 is used (hence, no CFL condition is initially enforced, but the time step is taken small enough). Typical values are $\Delta t^0 = 10^{-4}$s for the initial time step, and $\Delta Y = 10^{-4}$.

The solution to (4.4), (4.5), (4.6) is obtained as follows. We can solve the system (4.4) together with the boundary conditions (4.6a), (4.6c), for any value of b^{n+1} to evaluate the right-hand side (recall that the advective derivative is treated explicitly). This leads to a tridiagonal linear system whose system matrix results only from the time derivative and the diffusive terms. This matrix, which is diagonally dominant, has an inverse with nonnegative entries. Thus, the solution $(U_j^{n+1})_{1\leq j\leq n_Y}$ can be expressed linearly with nonnegative coefficients in terms of the coefficients $(a_j^{n+1/2})_{1\leq j\leq n_Y}$ which appear on the right-hand side and which depend on the still unknown interface position b^{n+1}. According to (4.5) and since U_j^n is nondecreasing with respect to j, U_j^{n+1} is thus, for all $j = 1 \dots n_Y$, a nondecreasing continuous and piecewise linear function of b^{n+1}, with two different formulae corresponding to whether b^{n+1} is greater or smaller than b^n. In particular, the remaining boundary condition (4.6b), which is equivalent to $U_1^{n+1} = 0$ owing to (4.6a), determines a unique solution b^{n+1}, see Figure 8. The value of b^{n+1} can be computed explicitly by solving twice the linear system with two different right-hand sides and using linear interpolation. The first solve uses the right-hand side evaluated with the temporary value b^n for b^{n+1}, yielding a temporary value for U_1^{n+1}; if the obtained value is negative (left panel of Figure 8), the second solve is performed using the value h for b^{n+1}, otherwise, the value 0 is used (right panel of Figure 8). Once b^{n+1} is known, we recover the entire profile U_j^{n+1} for all $j = 1 \dots n_Y$ by linear interpolation.

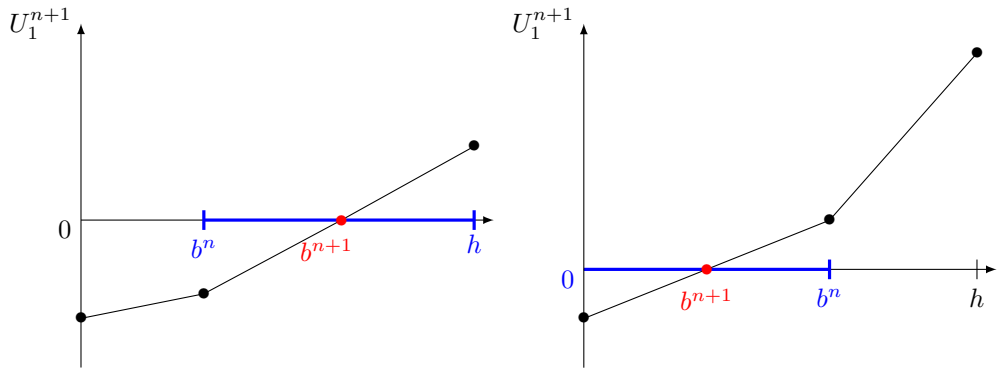

Figure 8: Velocity U_1^{n+1} versus b^{n+1}. The chosen value for b^{n+1} is determined by the intersection of the curve with the horizontal axis.

4.2 Discretization by optimality condition

The second numerical method for solving (2.5), (2.6), (2.7) with positive viscosity $\nu > 0$ uses a formulation as an optimal problem set on the whole interval $(0, h)$, valid under assumption (2.9),

$$\begin{cases} \min(\partial_t U + S - \nu \partial^2_{ZZ} U, U) = 0 & \text{for all } Z \in (0, h), \\ \partial_Z U = 0 & \text{at } Z = h, \\ U = 0 & \text{at } Z = 0, \end{cases} \tag{4.8}$$

where we consider a no-slip boundary condition at the bottom. Note that this condition becomes relevant whenever the static/flowing interface reaches the bottom, a situation encountered in our simulations as reflected in Figure 10c. In (4.8), the static/flowing interface position $b(t)$ no longer appears explicitly, but has to be deduced from the velocity profile as

$$b(t) = \sup \{ Z_0 \in [0, h] \text{ such that } U(t, Z) = 0 \text{ for all } Z \in [0, Z_0] \}. \tag{4.9}$$

We split the space domain $(0, h)$ in n_Z cells of length ΔZ with $n_Z \Delta Z = h$, and denote by $Z_j = (j - 1/2)\Delta Z$, for all $j = 1 \dots n_Z$, the center of the cells. The discrete times t^n, for all $n \geq 0$ are related by $t^{n+1} = t^n + \Delta t^n$, where Δt^n is the time step (chosen according to the CFL condition (4.12) below) and $t^0 = 0$. We discretize the problem (4.8) using a finite difference scheme by writing for the discrete unknowns $U_j^n \simeq U(t^n, Z_j)$

$$\min \left(\frac{U_j^{n+1} - U_j^n}{\Delta t^n} + S(t^n, Z_j) - \nu \frac{U_{j+1}^n + U_{j-1}^n - 2U_j^n}{\Delta Z^2}, U_j^{n+1} \right) = 0 \tag{4.10}$$

for all $j = 1 \dots n_Z$. The boundary conditions, which are discretized as $U_{n_Z+1}^n = U_{n_Z}^n$ at the free surface ($Z = h$) and as $U_0^n = -U_1^n$ at the bottom ($Z = 0$), are used to provide the ghost values involved in the discretization of the diffusive term. The problem (4.10) is solved in two steps as

$$\frac{U_j^{n+1/2} - U_j^n}{\Delta t^n} + S(t^n, Z_j) - \nu \frac{U_{j+1}^n + U_{j-1}^n - 2U_j^n}{\Delta Z^2} = 0, \qquad U_j^{n+1} = \max(U_j^{n+1/2}, 0). \tag{4.11}$$

Owing to the explicit discretization of the diffusive term, we use the CFL condition

$$2\nu \frac{\Delta t^n}{\Delta Z^2} \leq 1. \tag{4.12}$$

We could also consider an implicit discretization to avoid any CFL condition, but each time step would be more computationally demanding. Finally, the thickness of the static layer is evaluated as

$$b^n = \max \{ j \in \{1 \dots n_Z\} \text{ such that } U_k^n = 0 \text{ for all } k \in \{1 \dots j\} \} \times \Delta Z. \tag{4.13}$$

However, in order to avoid that b^n is influenced by small values of U, we prefer to use

$$b^n = (k^n - 1)\Delta Z, \qquad k^n = \min \left\{ j \in \{1, \dots, n_Z\} \text{ such that } U_j^n \geq C_0 \Delta Z^2 \right\}, \tag{4.14}$$

where C_0 is an appropriate constant of the order of S/ν, see (2.13).

4.3 Scales in the transient regime

We assume that the source term S is constant. Then, the solution to the viscous model (2.5), (2.6), (2.7) depends on the constant S, the total width h, the viscosity ν, the initial width of the static layer b^0, and the initial velocity profile $U^0(Z)$. We introduce non-dimensional quantities, denoted by hats, as

$$t = \tau \widehat{t}, \quad Z = l \widehat{Z}, \quad h = l \widehat{h}, \quad b = l \widehat{b}, \quad U = u \widehat{U}, \tag{4.15}$$

with τ a time scale, l a space scale, and $u = l\alpha_1$ where α_1 is the order of magnitude of the initial shear rate. In order to write (2.5) in non-dimensional form, we take

$$l = \nu\frac{\alpha_1}{S}, \qquad \tau = \frac{l^2}{\nu} = \nu\frac{(\alpha_1)^2}{S^2}. \tag{4.16}$$

The dimensionless equation is then

$$\partial_{\widehat{t}}\widehat{U} + 1 - \partial^2_{\widehat{Z}\widehat{Z}}\widehat{U} = 0 \quad \text{ for all } \widehat{Z} \in (\widehat{b}, \widehat{h}),$$

with boundary conditions $\widehat{U} = \partial_{\widehat{Z}}\widehat{U} = 0$ at $\widehat{Z} = \widehat{b}$, and $\partial_{\widehat{Z}}\widehat{U} = 0$ at $\widehat{Z} = \widehat{h}$. If we take a linear initial velocity profile, this non-dimensional solution $\widehat{U}$ depends only on $\widehat{h} = h/l$ and $\widehat{b}^0 = b^0/l$. Actually, since the problem is invariant by translation in Z, the solution depends only on $(h - b^0)/l$.

Numerical investigations for constant source S using the scheme described in Subsection 4.1 show the behavior illustrated in Figure 9. The static/flowing interface position $b(t)$ first decreases until a time $t^{\rm c}$ and attains a minimal value $b^{\min}$ (starting phase). Then, $b(t)$ increases, and (if h is sufficiently large) reaches an asymptotic regime with upward velocity $\dot{b}^\infty$ (stopping phase), before fully stopping at attaining h.

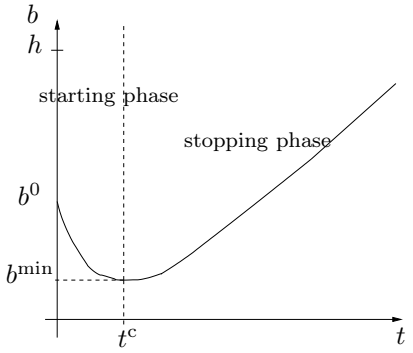

Figure 9: Evolution of the thickness of the static/flowing interface as a function of time.

According to the above scaling analysis, if the velocity profile is initially linear with shear α_1, and if

$$\frac{h - b^0}{l} = \frac{(h - b^0)S}{\nu\alpha_1} \gg 1, \tag{4.17}$$

the quantities $t^{\rm c}$, $b^0 - b^{\min}$, $\dot{b}^\infty$ are proportional to τ, l, l/τ, respectively. We obtain the proportionality factors from the numerical simulation as

$$t^{\rm c} = 0.15\nu\frac{(\alpha_1)^2}{S^2}, \qquad b^0 - b^{\min} = 0.43\nu\frac{\alpha_1}{S}, \qquad \dot{b}^\infty = 0.95\frac{S}{\alpha_1}. \tag{4.18}$$

Note the dependency in the ratio α_1/S, which is due to the homogeneity of the problem (2.5), (2.6) with respect to (U, S) (multiplying (U, S) by a positive constant gives again a solution, with b unmodified).

4.4 Results and comparison with experiments for constant viscosity

We consider the case of a constant and uniform source term of the form (3.3). The case of a linear initial velocity profile is simulated using different values of the viscosity ν (taken constant) and slope angles θ. The results obtained with both methods of Subsections 4.1 and 4.2 are always identical, thus we shall not specify which one is used. As discussed in Subsection 4.3, the static/flowing interface always penetrates the initially static layer, in

contrast to what has been observed for the inviscid case, within a length $b^0 - b^{\min}$ proportional to ν, according to (4.18). In other words, the flow excavates the static bed. However, for $\nu < 10^{-5}\mathrm{m}^2\mathrm{s}^{-1}$, the penetrating length is too small to be observable. For $\nu = 10^{-5}\mathrm{m}^2\mathrm{s}^{-1}$ (Figure 10a), $b^0 - b^{\min} = 8 \cdot 10^{-4}$m for $\theta = 24^o$ (with $t^c = 5 \cdot 10^{-2}$s), and $b^0 - b^{\min} = 2 \cdot 10^{-4}$m for $\theta = 19^o$ (with $t^c = 4 \cdot 10^{-3}$s). Thus, the static/flowing interface penetrates only slightly within the initially static layer. As the viscosity increases (Figure 10b), the static/flowing interface penetrates deeper into the initially static layer and even reaches the bottom for $\nu = 10^{-4}\mathrm{m}^2\mathrm{s}^{-1}$ at $\theta = 24^o$ (Figure 10c). The results that better reproduce the experimental observation for the penetration of $b(t)$ within the initially static layer are obtained with $\nu \simeq 5 \cdot 10^{-5}\mathrm{m}^2\mathrm{s}^{-1}$. In good agreement with the experiments, the simulations with viscosity predict that the static/flowing interface sinks deeper within the initially static layer and for a longer time t^c when the slope angle increases. Furthermore, the values of $b(t)$ and t^c are in reasonable agreement with those observed experimentally (Figures 2 and 10b and Figure 17 of [12]).

Qualitatively similar results are obtained using different initial velocity profiles (Figure 12). However, the shape of $b(t)$ is affected by the choice for the initial velocity profile. As an example, for an exponential initial velocity profile with $\theta = 24^o$ and $\nu = 5 \cdot 10^{-5}\mathrm{m}^2\mathrm{s}^{-1}$, the static/flowing interface position $b(t)$ stagnates at an almost constant position for the first 0.5s, contrary to the case of a linear initial velocity profile (Figures 10b and 12b).

The convex shape of $b(t)$ during the migration of the static/flowing interface up to the free surface obtained in the viscous case is very different from the observation and from that obtained in the inviscid case, which predicted a linear shape related to the linear initial velocity profile. In the viscous case, the time evolution of $b(t)$ and the velocity profile $U(t, Z)$ are not so obviously related to the shape of the initial velocity profile, as shown for example in Figure 12 for $\theta = 24^o$. The velocity profiles in the viscous case are also very different from those in the inviscid case. Whatever the shape of the initial velocity profile, at later time, the velocity profiles exhibit an exponential-like tail near the static/flowing interface, similar to that observed experimentally. They also exhibit a convex shape near the free surface which can be observed in some experimental velocity profiles, but not always and not as marked (e.g., Figure 3c). While the maximum velocity decreases too fast at $t = 0.5$s and $\theta = 24^o$ compared to the experiments and to the inviscid case, the velocity is much closer to the experiments at $t = 1$s than in the inviscid case (Figure 3c and Figure 11c). For $\theta = 19^o$ and $\theta = 22^o$, the viscous case overestimates the decrease in velocity at time $t = 0.7$s.

Finally, the stopping time of the whole granular layer is smaller for viscous than for inviscid flow, whatever the shape of the initial velocity profile. Recalling that the stopping time in the inviscid case is given by $t^{\mathrm{stop}}_{\nu=0} = U^0(h)/S$, we can study numerically the difference $(t^{\mathrm{stop}}_{\nu=0} - t^{\mathrm{stop}}_{\nu})$, where t^{stop}_{ν} denotes the stopping time in the viscous case. Our numerical simulations show that this difference depends rather mildly on the viscosity (Figure 13 where the slope of the curves suggests a behavior of this difference close to $\nu^{1/4}$ for the present parameters). In any case, the presence of viscosity diminishes the stopping time. Furthermore, the stopping time in the viscous case is significantly smaller than in the experiments.

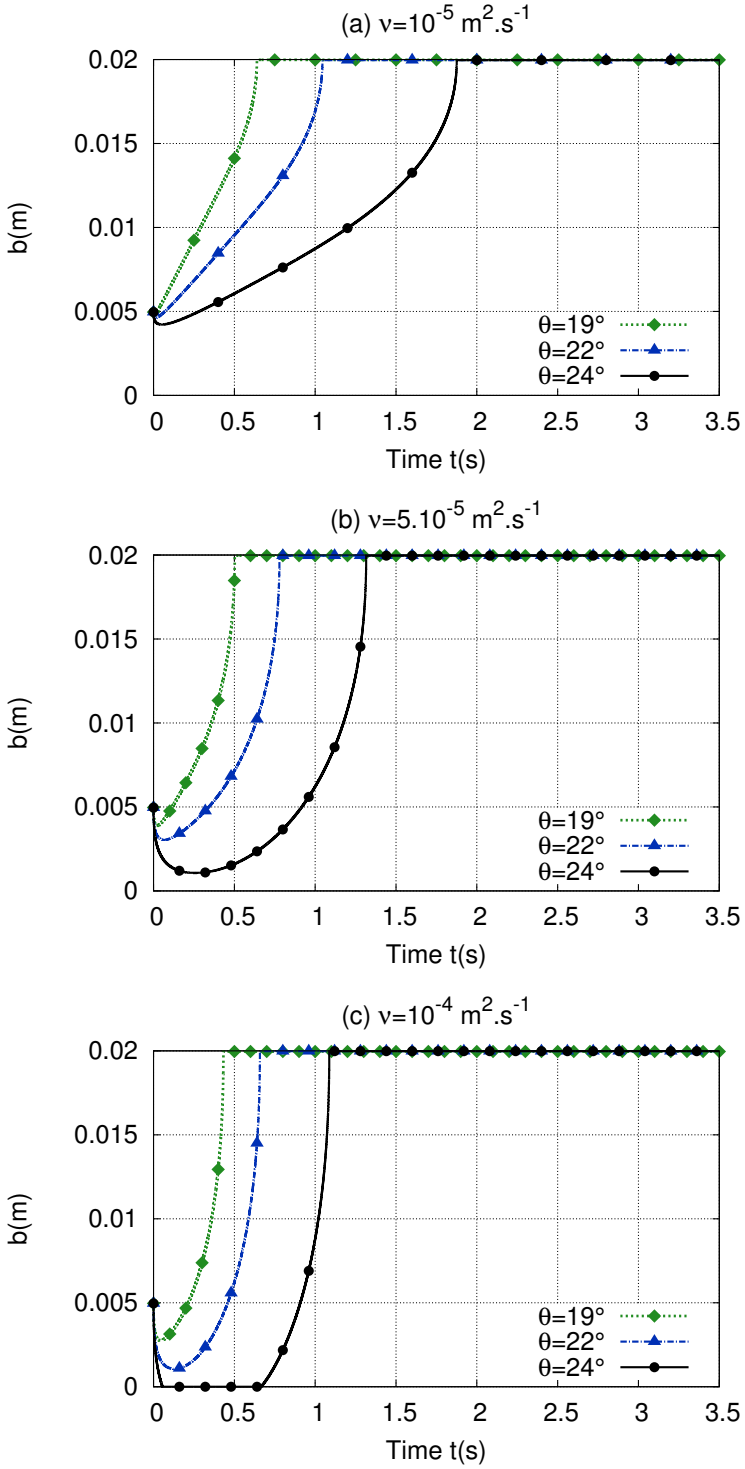

Figure 10: Static/flowing interface position b as a function of time t for different slope angles using a linear velocity profile, and different viscosities (a) $\nu = 10^{-5}\mathrm{m}^2\mathrm{s}^{-1}$, (b) $\nu = 5\cdot10^{-5}\mathrm{m}^2\mathrm{s}^{-1}$, and (c) $\nu = 10^{-4}\mathrm{m}^2\mathrm{s}^{-1}$.

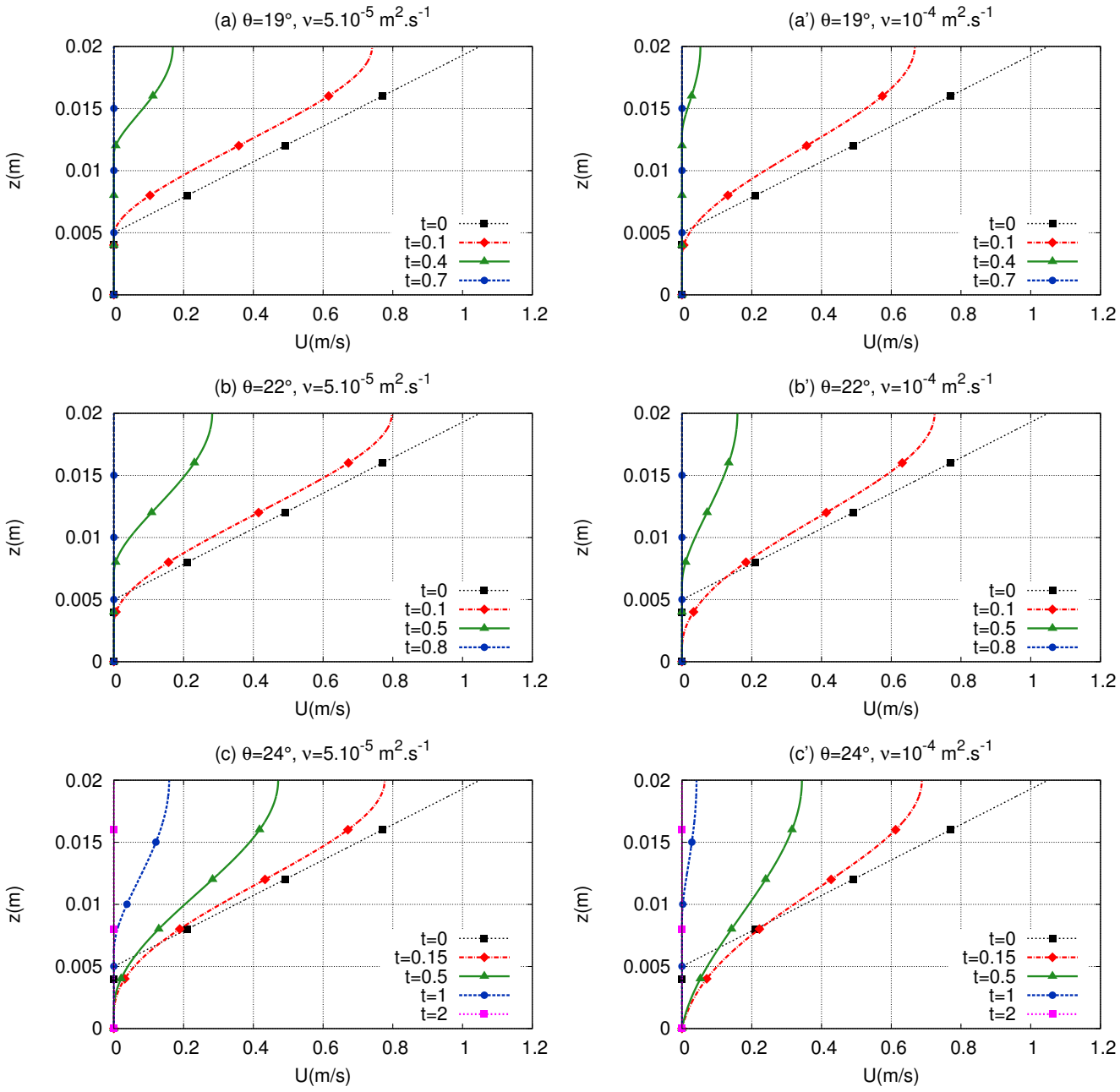

Figure 11: Velocity profiles $U(Z)$ at different times, with a linear velocity profile, for two different viscosities (a-b-c) $\nu = 5 \cdot 10^{-5}\mathrm{m}^2\mathrm{s}^{-1}$ and (a'-b'-c') $\nu = 10^{-4}\mathrm{m}^2\mathrm{s}^{-1}$, and for the slope angles (a-a') $\theta = 19^o$, (b-b') $\theta = 22^o$, and (c-c') $\theta = 24^o$.

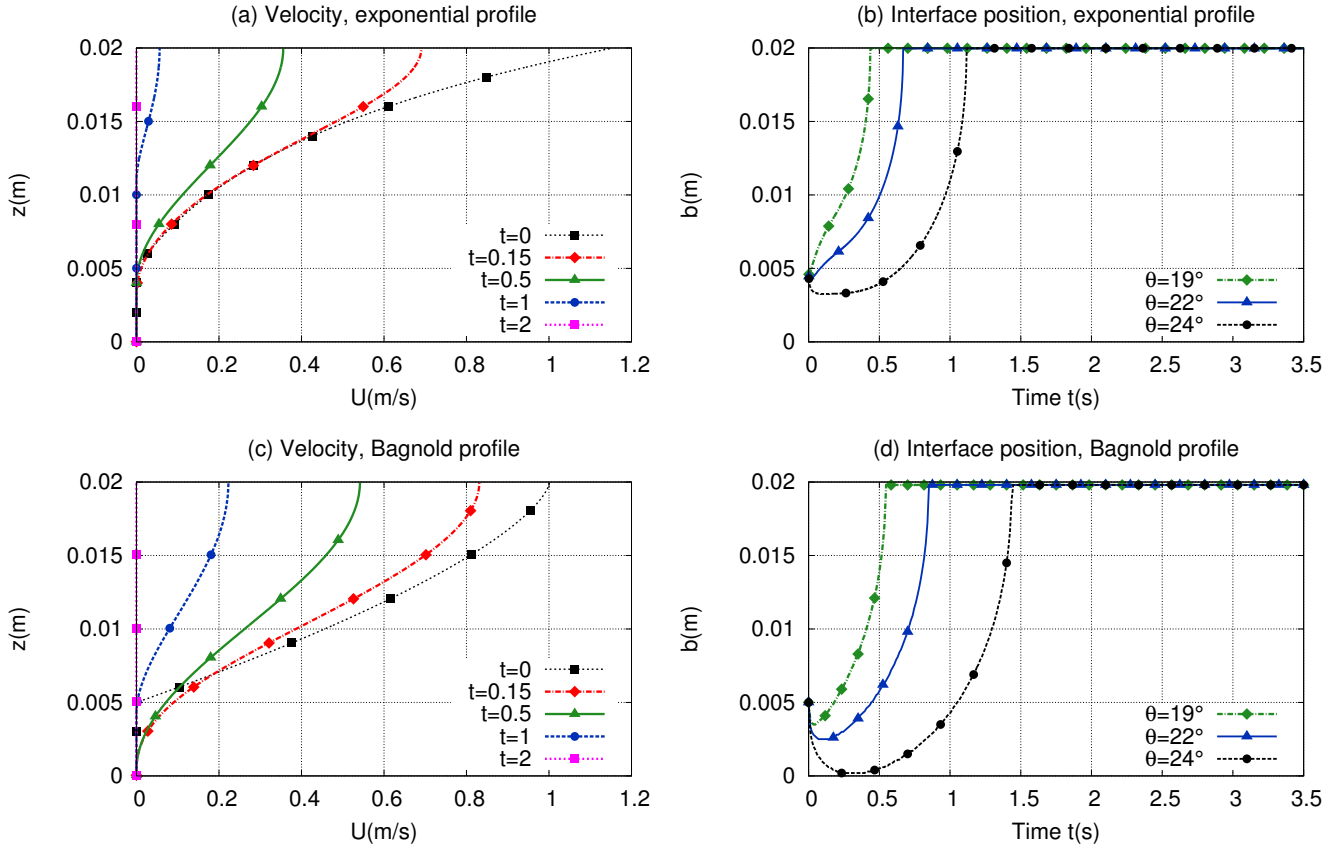

Figure 12: (left) Velocity profiles $U(Z)$ and (right) evolution of the thickness of the static/flowing interface position b, with an inclined plane of slope $\theta = 24^o$ and a viscosity $\nu = 5 \cdot 10^{-5}\mathrm{m}^2\mathrm{s}^{-1}$, using (a-b) an exponential and (c-d) a Bagnold initial velocity profile.

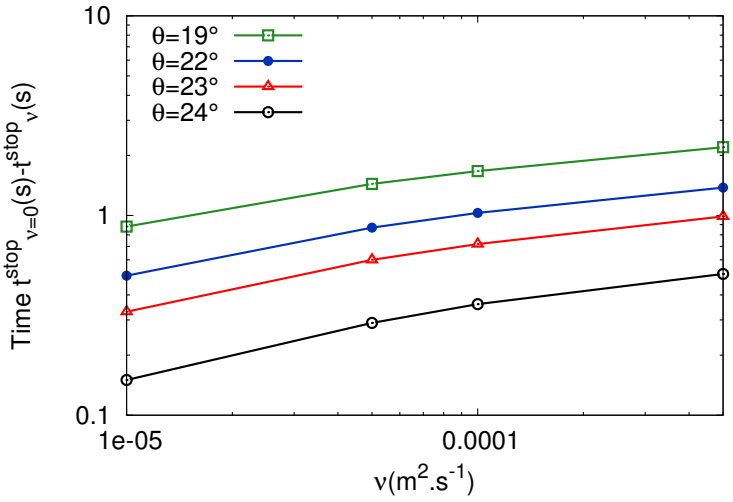

Figure 13: $t^{\mathrm{stop}}_{\nu=0} - t^{\mathrm{stop}}_{\nu}$ with respect to the viscosity in log scale.

4.5 Variable viscosity

The viscoplastic description of granular materials involves fundamentally a Drucker-Prager yield stress proportional to the pressure, the coefficient being the static friction coefficient $\mu_s = \tan\delta$. A full rheological law including this yield stress (i.e., defined for all values of the strain rate and not only close to zero) has been proposed in [21], the so called $\mu(I)$ rheology. As described in [16], this rheology can be interpreted as a decomposition (i.e., (2.1)) of the deviatoric stress tensor in a rate independent pure plastic part proportional to μ_s, and a viscous part with pressure and rate dependent dynamic viscosity η given by

$$\eta = (\mu(I) - \mu_s)\frac{p_{dyn}}{2\|D\|}, \tag{4.19}$$

where p_{dyn} is the dynamic pressure, D is the strain rate tensor, $\|D\|^2 = \frac{1}{2}\sum_{ij} D_{ij}^2$, and I is the inertial number defined by

$$I = \frac{2\|D\|d}{\sqrt{p_{dyn}/\rho_s}}, \tag{4.20}$$

with d the grain diameter as before, and ρ_s the grain density. The kinematic pressure p is related to p_{dyn} by $p = p_{dyn}/\rho$, with $\rho = \phi\rho_s$ the density of the granular material, ϕ being the volume fraction. If we consider a slope aligned velocity field depending only on the normal variable Z, the same computation as in [6] shows that the system (2.5), (2.6), (2.7) is modified only by the definition of viscosity, namely it becomes

$$\partial_t U(t,Z) + S - \partial_Z\big(\nu\partial_Z U(t,Z)\big) = 0 \quad \text{for all } Z \in (b(t), h), \tag{4.21}$$

with the same boundary and initial conditions (2.6), (2.7), the constant and uniform source term S given by (3.3), and $\nu = \eta/\rho$. In such flow one has hydrostatic pressure $p = g\cos\theta(h - Z)$, and shear rate $\|D\| = \partial_Z U/2$. Thus with (4.19), the kinematic viscosity becomes

$$\nu = (\mu(I) - \mu_s)\frac{g\cos\theta(h-Z)}{\partial_Z U}, \tag{4.22}$$

with

$$I = \frac{\partial_Z U d}{\sqrt{\phi g\cos\theta(h-Z)}}. \tag{4.23}$$

Then the term appearing in (4.21) is

$$\nu\partial_Z U = (\mu(I) - \mu_s)g\cos\theta(h - Z), \tag{4.24}$$

and the part of this term proportional to μ_s indeed balances in (4.21) the corresponding part in S from (3.3). The nonlinearity is given according to [21] as

$$\mu(I) = \mu_s + (\mu_2 - \mu_s)\frac{I}{I + I_0}, \tag{4.25}$$

with $\mu_2 > \mu_s$ the friction at large strain rate, and $I_0 = 0.279$. We note that the boundary condition (2.6c) is automatically satisfied, we can thus just skip it.

For the discretization we use the method of Subsection 4.2 with the discrete unknowns $U_j^n \simeq U(t^n, Z_j)$, $Z_j = (j - 1/2)\Delta Z$ for $j = 1 \dots n_Z$, $n_Z\Delta Z = h$. The equations (4.21), (4.24) with (4.25), (4.23) are discretized with finite differences under conservative form

$$\frac{U_j^{n+1/2} - U_j^n}{\Delta t^n} + S(t^n, Z_j) - \frac{\Phi_{j+1/2}^n - \Phi_{j-1/2}^n}{\Delta Z} = 0, \tag{4.26}$$

for all $j = 1 \dots n_Z$, with

$$\Phi_{j+1/2}^n = (\mu(I_{j+1/2}) - \mu_s)g\cos\theta(h - Z_{j+1/2}), \qquad I_{j+1/2} = \frac{d\,(U_{j+1}^n - U_j^n)/\Delta Z}{\sqrt{\phi g\cos\theta(h - Z_{j+1/2})}} \tag{4.27}$$

for $j = 0 \dots n_Z$, with $Z_{j+1/2} = Z_j + \Delta Z/2 = j\Delta Z$, and then

$$U_j^{n+1} = \max(U_j^{n+1/2}, 0). \tag{4.28}$$

Since $\Phi^n_{n_Z+1/2} = 0$, there is no need to define $U^n_{n_Z+1}$, in accordance with the loss of the free surface boundary condition (2.6c). On the left boundary (bottom) we use as before the no-slip condition, $U_0^n = -U_1^n$. We use the CFL condition $2\nu_{\max}\Delta t^n \leq \Delta Z^2$, with $\nu_{\max}$ defined as the maximum value of ν computed with (4.22). The interface position b^n is computed according to (4.14).

As previously we take $\mu_s = \tan(26^o)$, $h = 0.02$m, $b^0 = 0.005$m, $d = 7 \cdot 10^{-4}$m, and following [12] $\phi = 0.62$. We choose $\mu_2 = \tan(28^o)$, that leads to $\nu(Z = b^0) \simeq 5 \cdot 10^{-5}\text{m}^2\text{s}^{-1}$, corresponding to the order of magnitude of ν taken in Subsection 4.4. We consider the case of a linear initial velocity profile, with slope angles $\theta = 19^o, 22^o, 24^o$. The numerical results for the static/flowing interface position $b(t)$ and velocity profiles $U(Z)$ are plotted in Figures 14 and 15. In comparison with the constant viscosity numerical results of Figures 10(b) and 11(a-b-c), the shapes are similar, in particular for the initial erosion of the static bed. The behavior of the interface position $b(t)$ reaching the free surface close to the stopping time is here closer to the inviscid case of Figure 5(a), but however does not recover the expected (since ν vanishes at the free surface) roughly linear behavior of the experimental results of Figure 2. For clarity, the static/flowing interfaces and the velocity profiles corresponding to the different cases are plotted in Figure 16.

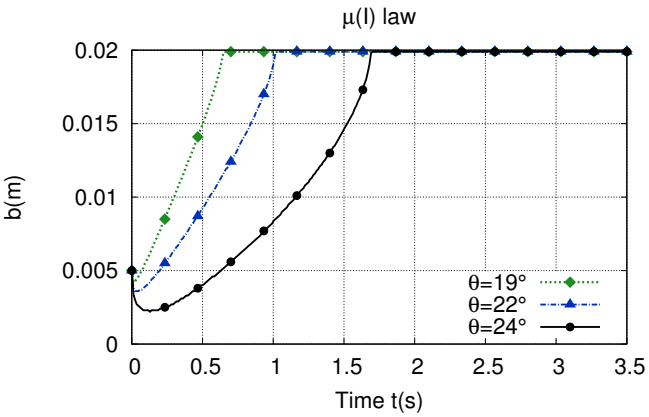

Figure 14: Static/flowing interface position b as a function of time t, for variable viscosity associated with the $\mu(I)$ law, with linear initial velocity profile and slope angles $\theta = 19^o$, $\theta = 22^o$, $\theta = 24^o$.

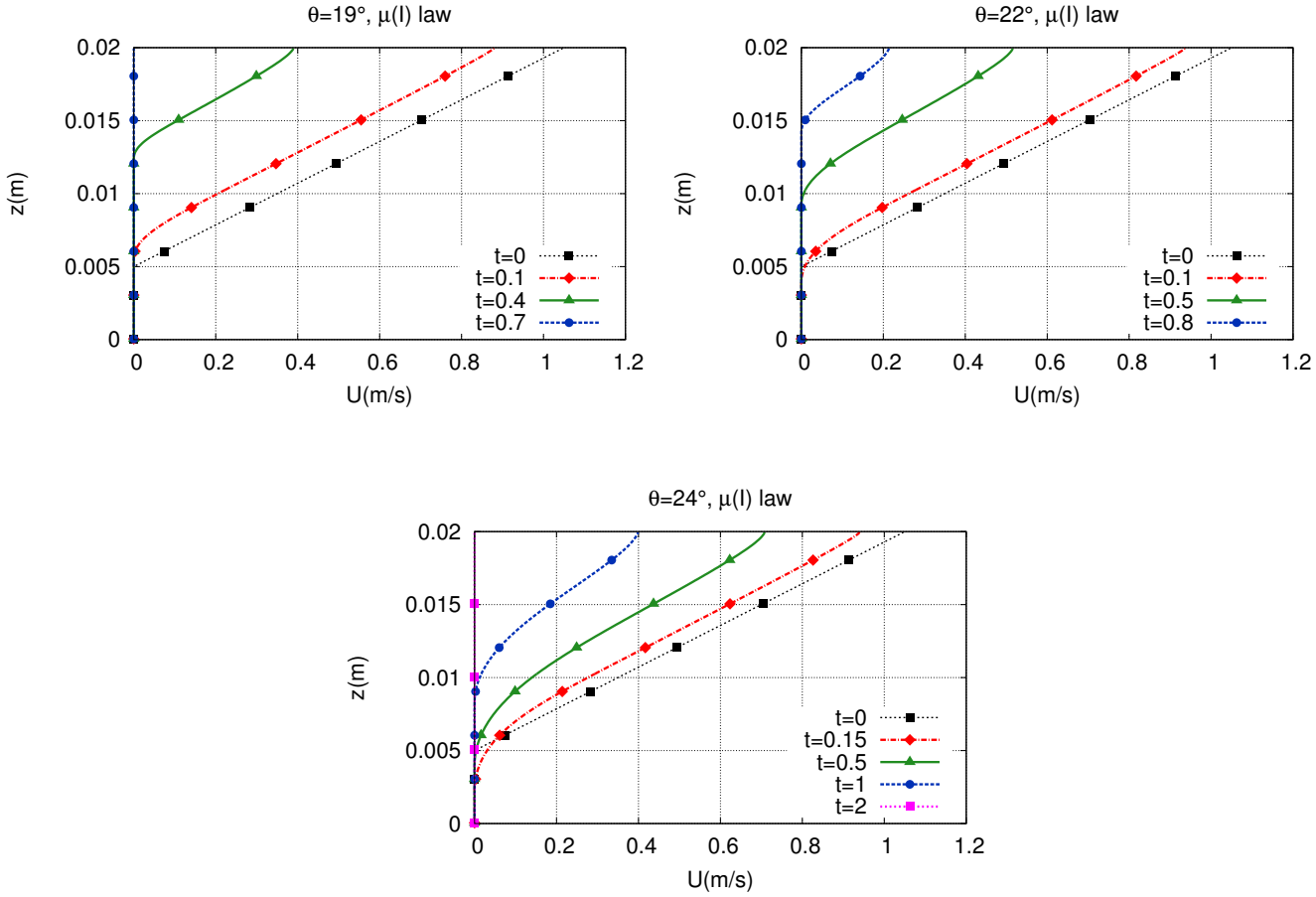

Figure 15: Velocity profiles $U(Z)$ at different times, for variable viscosity associated with the $\mu(I)$ law, with linear initial velocity profile and slope angles $\theta = 19^o$, $\theta = 22^o$, $\theta = 24^o$.

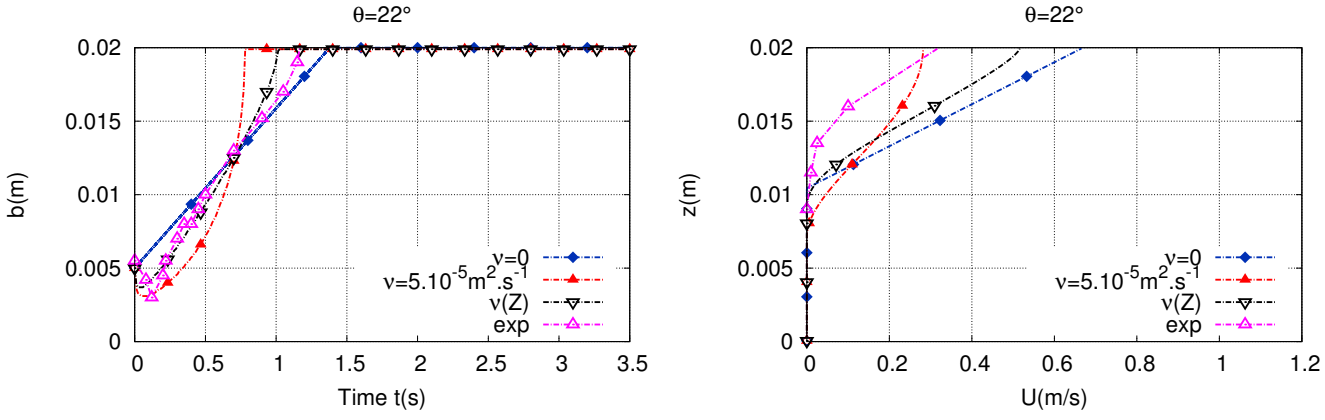

Figure 16: Static/flowing interface position b as a function of time t (left), and velocity profiles $U(Z)$ at time $t = 0.5$s (right), with linear initial velocity profile and slope angle $\theta = 22^o$, for respectively experimental measurements, our model without viscosity, with constant viscosity $\nu = 5 \cdot 10^{-5}\mathrm{m}^2\mathrm{s}^{-1}$, or variable viscosity associated with the $\mu(I)$ law.

It is important to explain the behavior of the solution close to the free surface. As said above, there is no need to impose any boundary condition at the free surface, because the pressure vanishes there. Nevertheless, the behavior close to the free surface of the solution to the parabolic problem (4.21) is deduced from the property that $\partial_Z(\nu\partial_Z U)$ is bounded, which gives that $\nu\partial_Z U \sim h - Z$. In the case of constant viscosity it leads to $\partial_Z U \sim h - Z$, and U has a roughly parabolic profile close to the free surface. In the case of $\mu(I)$ rheology, (4.24) gives that I tends to a finite value as $Z \to h$, and thus with (4.23) we obtain $\partial_Z U \sim \sqrt{h - Z}$, and U has a rough Bagnold profile close to the free surface. We conclude that in any case the Neumann condition $\partial_Z U = 0$ is recovered at the free surface, even if not imposing it. In the case of the $\mu(I)$ rheology, $\partial_Z U$ tends to zero more slowly than in the case of constant viscosity, giving a behavior closer to the inviscid case. Nevertheless, this property $\partial_Z U = 0$ at the free surface, that seems to be consequence of the incompressible viscoplastic model, prevents a good representation of the experimental stopping phase. It is noticeable that the $\mu(I)$ rheology has been introduced exactly in order to represent the Bagnold profile (without static phase) $U(Z) = c(h^{3/2} - (h - Z)^{3/2})$, where c is determined by the relation $\mu(I) = \tan\theta$. It is a solution to the system (4.21), (4.24) with (4.25), (4.23), but in the situation when $\mu_s < \tan\theta < \mu_2$, which does not correspond to our framework of progressive stopping, i.e., when $\tan\theta < \mu_s$.

5 Discussion and conclusion

We have proposed here a 1D (in the direction normal to the flow) thin-layer model with static/flowing dynamics based on the description of a granular material by a yield stress viscoplastic rheology. In this model, the flow thickness is constant. We have compared model solutions for both the inviscid and viscous cases to observations from experiments on granular flow over an inclined static layer of grains. The analytical solution for the inviscid case and the numerical results for the viscous case reproduce quantitatively some essential features of the change with time of the velocity, of the static/flowing interface position, and of the stopping time of the granular mass, even though the flow thickness in the experiments is not perfectly uniform and the initial velocity profile changes with slope angle and flow thickness.

The analytical solution for the inviscid case shows that the evolution of the static/flowing interface position is proportional to the source term and inversely proportional to the shear rate (equation (2.15)). For the viscous case (with constant viscosity), the analysis of the model shows that the evolution of the interface is related to the viscosity, the source term, and the first and third derivative of the source term and the velocity, respectively (equation (2.14)). Due to the appearance of this third derivative, the dynamics of the static/flowing interface cannot be reduced to a simple differential equation in terms of depth-averaged quantities. While the shape of the initial velocity profile is preserved at all times in the inviscid case according to (3.4), an exponential-like tail near the static/flowing transition and a convex shape near the free surface develop in the viscous case. The viscous contribution enables the static/flowing interface to initially penetrate within the static layer (which is eroded), as observed in the experiments, as opposed to the inviscid case.

The viscoplastic model used here has the great advantage of involving only two parameters, i.e., the friction coefficient μ_s and the viscosity ν (or the coefficient μ_2 in the case of the $\mu(I)$ rheology), while the so-called partial fluidization theory, involving an order parameter to describe the transition between static and flowing material, also reproduces the erosion of the static bed and the velocity profiles obtained here in the viscous case [27], but at the cost of additional empirical equations for the time-change of a state parameter.

One of the important results of the analysis lies in the explicit expressions obtained from the analytical solution, especially for the time evolution of the static/flowing interface. The dynamics are controlled by the source term S that is constant when hydrostatic pressure is assumed and when the slope and thickness are assumed to be constant. In such a case, $S(t, Z) = S = g\cos\theta(\tan\delta - \tan\theta)$. Comparable results have been obtained from the an-

alytical solution of shallow depth-averaged equations for a granular dam-break (i.e., with non-constant h) [26, 11]. This analytical solution predicts a granular mass front velocity that decreases linearly with time

$$U_f = \max\left(2\sqrt{kgh_0\cos\theta} - (g\cos\theta(\tan\delta - \tan\theta)\,t, 0\right), \tag{5.1}$$

where $k \simeq 0.5$ (see [28]). Furthermore, the stopping time of the analytical front for the granular dam-break is

$$t_f = 2\sqrt{\frac{kh_0}{g\cos\theta}}\frac{1}{\tan\delta - \tan\theta}. \tag{5.2}$$

Equations (5.1), (5.2) for the front velocity and the stopping time of the front for a depth-averaged model of a granular dam-break are very similar to equations (3.4) and (3.6) respectively, found here for the velocity of the flow and for the stopping time of the granular layer in the non-averaged case and without viscosity.

Although the initial penetration of the static/flowing interface into the static layer (erosion) can be reproduced by taking into account the viscosity, this leads at the same time to an underestimation of the stopping time. The viscous model better reproduces the exponential-like tail of the velocity profile near the static/flowing interface than the inviscid model, but overestimates the convexity of the velocity profile near the free surface. Furthermore, the change in shape of the velocity profile observed in the experiments during the stopping phase is reproduced in the viscous case, as opposed to the inviscid case, but the decrease in maximum velocity near the surface is too fast in the viscous case. All these results suggest that (i) viscosity plays an important role near the static/flowing interface at depth and in this region a reasonable estimate for the viscosity is $\nu \simeq 5\cdot 10^{-5}\mathrm{m}^2\mathrm{s}^{-1}$ and (ii) viscous effects in the experiments seem to be much smaller near the free surface. These observations suggest a non-constant viscosity, as proposed in the so-called $\mu(I)$ flow law, e.g., [14, 33, 20, 21]. Following [16], we have used the $\mu(I)$ flow law to derive the value of the viscosity, which becomes variable and nonlinear with respect to the shear rate. This flow law reproduces the value of the viscosity at the static/flowing interface (i.e., $\nu \simeq 5\cdot 10^{-5}\mathrm{m}^2\mathrm{s}^{-1}$) and at the free surface (vanishing viscosity). However, this modeling does not allow us to significantly improve the accuracy of the behavior of the static/flowing interface close to stopping. This is because it imposes a Bagnold behavior close to the free surface, which is in contradiction with experiments that predict a linear behavior.

It would be of interest to take into account the X-variations of the source S from (2.4), thereby accounting for topography, propagation and non-hydrostatic effects. The influence of a Z-dependency of S on the static/flowing interface dynamics and on the erosion process in the simplified model (2.5), (2.6), (2.7) has been studied in [25]. It would be interesting to extend the approach proposed here to 2D and possibly 3D, so as to capture the static/flowing interface in shallow models, as proposed in [6]. The orders of magnitude assumed in [6] are indeed satisfied in the experiments discussed here, because the typical length is $L = 1\mathrm{m}$, typical time $\tau = 0.33\mathrm{s}$ satisfying $L/\tau^2 = g$, $h = 0.02\mathrm{m}$, $\nu = 5\cdot 10^{-5}\mathrm{m}^2\mathrm{s}^{-1}$, leading to $\varepsilon \equiv h/L = 0.02$, $\tan\delta - \tan\theta = O(\varepsilon)$, and the normalized viscosity $\nu\tau/L^2 \simeq 10^{-5}$ is of the order of ε^2 or ε^3. The primary models of [6] lead however to severe nonlinearities, so that these extensions with flow-aligned variations represent a major challenge to treat numerically.

An important issue is also to summarize the dynamics of the normal velocity profile using a finite number of parameters (for example interface position b, width h, and shear rate), in order to keep computational costs low enough to simulate natural situations. This could lead to a depth-averaged model, which has until now seemed inaccessible because of the dependency on the third normal derivative in the differential equation (2.14).

Acknowledgments

The authors are thankful to Maxime Farin and Olivier Roche for sharing new results from the experiments performed by [12] and [13], to Maxime Farin for helping extract the specific

results presented here from these experiments, and to Régis Monneau for stimulating discussions on the discretization by an optimality condition. This work has been partially funded by the ANR contract ANR-11-BS01-0016 LANDQUAKES, by the Labex Bézout, and by the ERC contract ERC-CG-2013-PE10-617472: ERC SLIDEQUAKES.

References

[1] T. Barker, D.G. Schaeffer, P. Bohorquez, J.M.N.T Gray, *Well-posed and ill-posed behaviour of the mu(I)-rheology for granular flows*, *J. Fluid Mech.*, submitted, 2015.

[2] C. Berger, B.W. McArdell, F. Schlunegger, *Direct measurement of channel erosion by debris flows, Illgraben, Switzerland*, *J. Geophys. Res.*, 116:F01002, 2011.

[3] F. Bouchut, M. Westdickenberg, *Gravity driven shallow water models for arbitrary topography*, *Commun. Math. Sci.*, 2:359-389, 2004.

[4] F. Bouchut, A. Mangeney-Castelnau, B. Perthame, J.-P. Vilotte, *A new model of Saint Venant and Savage-Hutter type for gravity driven shallow water flows*, *C. R. Math. Acad. Sci. Paris*, 336:531-536, 2003.

[5] F. Bouchut, E.D. Fernández-Nieto, A. Mangeney, P.-Y. Lagrée, *On new erosion models of Savage-Hutter type for avalanches*, *Acta Mech.*, 199:181-208, 2008.

[6] F. Bouchut, I. Ionescu, A. Mangeney, *An analytic approach for the evolution of the static-flowing interface in viscoplastic granular flows*, hal-01081213, https://hal.archives-ouvertes.fr/hal-01081213v2, 2014.

[7] S.J. Conway, A. Decaulne, M.R. Balme, J.B. Murray, M.C. Towner, *A new approach to estimating hazard posed by debris flows in the Westfjords of Iceland*, *Geomorphology*, 114:556-572, 2010.

[8] G.B. Crosta, S. Imposimato, D. Roddeman, *Numerical modeling entrainment/deposition in rock and debris-avalanches*, *Eng. Geol.*, 109:135-145, 2009.

[9] G.B. Crosta, S. Imposimato, D. Roddeman, *Numerical modeling of 2-d granular step collapse on erodible and non-erodible surface*, *J. Geophys. Res.-Earth surface*, 114:F03020, 2009.

[10] S. Deboeuf, O. Dauchot, L. Staron, A. Mangeney, J.-P. Vilotte, *Memory of the unjamming transition during cyclic tiltings of a granular pile*, *Phys. Rev. E*, E72:051305, 2005.

[11] G. Faccanoni, A. Mangeney, *Exact solution for granular flows*, *Int. J. Num. Analy. Meth. Goemech.*, 37:1408-1433, 2013.

[12] M. Farin, A. Mangeney, O. Roche, *Fundamental changes of granular flow dynamics, deposition, and erosion processes at high slope angles: insights from laboratory experiments*, *J. Geophys. Res. Earth Surf.*, 119:504-532, 2014.

[13] M. Farin, , PhD thesis, Institut de Physique du Globe de Paris, 2015.

[14] GDR-MiDi, *On dense granular flows*, *Eur Phys J E Soft Matter*, 14(4):341-365, 2004.

[15] O. Hungr, S.G. Evans, M.J. Bovis, J.N. Hutchinson, *Review of the classification of landslides of the flow type*, *Environ. Eng. Geosci.*, 7:221-238, 2001.

[16] I.R. Ionescu, A. Mangeney, F. Bouchut, O. Roche, *Viscoplastic modelling of granular column collapse with pressure dependent rheology*, *J. Non-Newtonian Fluid Mech.*, 2015.

[17] R.M. Iverson, M. Reid, M. Logan, R. LaHusen, J.W. Godt, J. Griswold, *Positive feedback and momentum growth during debris-flow entrainment of wet bed sediment*, Nat. Geosci., 4:116-121, 2011.

[18] R.M. Iverson, *Elementary theory of bed-sediment entrainment by debris flows and avalanches*, J. Geophys. Res., 117:F03006, 2012.

[19] R.M. Iverson, C. Ouyang, *Entrainment of bed material by Earth-surface mass flows: review and reformulation of depth-integrated theory*, Reviews of Geophysics, 53, doi: 10.1002/2013RG000447, 2015.

[20] P. Jop, Y. Forterre, O. Pouliquen, *Crucial role of sidewalls in dense granular flows: consequences for the rheology*, J. Fluid Mech., 541:167-192, 2005.

[21] P. Jop, Y. Forterre, O. Pouliquen, *A constitutive law for dense granular flows*, Nature, 441:727-730, 2006.

[22] D.V. Khakhar, A.V. Orpe, P. Andresén, J.M. Ottino, *Surface flow of granular materials: model and experiments in heap formation*, J. Fluid Mech, 441:225-264, 2001.

[23] P.-Y. Lagrée, L. Staron, S. Popinet, *The granular column collapse as a continuum: validity of a two-dimensional Navier-Stokes model with a $\mu(I)$-rheology*, J. Fluid Mech, 686:378-408, 2011.

[24] A. Lucas, A. Mangeney, J.-P. Ampuero, *Frictional velocity-weakening in landslides on Earth and on other planetary bodies*, Nature Communications, 5:3417, 2014.

[25] C. Lusso, *Modélisation numérique des écoulements gravitaires viscoplastiques avec transition fluide/solide*, PhD thesis. Université Paris-Est, Champs-sur-Marne, 2013.

[26] A. Mangeney, Ph. Heinrich, R. Roche, *Analytical and numerical solution of the dam-break problem for application to water floods, debris and dense snow avalanches*, Pure Appl. Geophys., 157:1081-1096, 2000.

[27] A. Mangeney, L.S. Tsimring, D. Volfson, I.S. Aranson, F. Bouchut, *Avalanche mobility induced by the presence of an erodible bed and associated entrainment*, Geophys. Res. Lett., 34:L22401, 2007.

[28] A. Mangeney, O. Roche, O. Hungr, N. Mangold, G. Faccanoni, A. Lucas, *Erosion and mobility in granular collapse over sloping beds*, JGR-Earth Surface, 115:F03040, 2010.

[29] A. Mangeney-Castelnau, F. Bouchut, J.-P. Vilotte, E. Lajeunesse, A. Aubertin, M. Pirulli, *On the use of Saint Venant equations to simulate the spreading of a granular mass*, J. Geophys. Res., 110:B09103, 2005.

[30] L. Moretti, A. Mangeney, Y. Capdeville, E. Stutzmann, C. Huggel Christian, D. Schneider, F. Bouchut, *Numerical modeling of the Mount Steller landslide flow history and of the generated long period seismic waves*, Geophys. Res. Lett., 39:L16402, 2012.

[31] P. Richard, A. Valance, J.-F. Metayer, P. Sanchez, J. Crassou, M. Louge, R. Delannay, *Rheology of confined granular flows: scale invariance, glass transition, and friction weakening*, Phys. Rev. Lett., 101:248002, 2008.

[32] S.B. Savage, K. Hutter, *The motion of a finite mass of granular material down a rough incline*, J. Fluid Mech., 199:177-215, 1989.

[33] L.E. Silbert, D. Ertas, G.S. Grest, T.C. Halsey, D. Levine, S.J. Plimpton, *Granular flow down an inclined plane: Bagnold scaling and rheology*, Phys. Rev. E, 64:051302, 2001.

[34] B. Sovilla, P. Burlando, P. Bartelt, *Field experiments and numerical modeling of mass entrainment in snow avalanches*, J. Geophys. Res., 111:F03007, 2006.

[35] N. Taberlet, P. Richard, A. Valance, R. Delannay, W. Losert, J.M. Pasini, J.T. Jenkins, *Super stable granular heap in thin channel*, *Phys. Rev. Lett.*, 91:264301, 2003.

[36] J.T. Weidinger, O. Korup, H. Munack, U. Altenberger, S.A. Dunning, G. Tippelt, W. Lottermoser, *Giant rockslides from the inside*, *Earth and Planetary Sci. Lett.*, 389: 62-73, 2014.